Electronic Supplementary Material (ESI) for Nanoscale.

Supporting information

Copper indium sulfide quantum dots enabling quantitative visible light photoisomerisation of (*E*)-azobenzene chromophores

Zakaria Ziani,[a] Caterina Bellatreccia,[a] Filippo Battaglia,[a] Giacomo Morselli,[a] Alessandro Gradone,[b] Paola Ceroni*[a] and Marco Villa*[a]

[a] University of Bologna, Dipartimento di Chimica Giacomo Ciamician, Via Selmi 2, 40126 Bologna, Italia

[b] Istituto per la Microelettronica ed i Microsistemi (IMM) – CNR Sede di Bologna, via Gobetti 101, 40129 Bologna, Italy

Contents

Determination of photoswitch loading on CIS-QDs surface 3

NMR spectra 4

(S)TEM Analysis 8

Absorption and emission spectroscopic data 10

- **Absorption spectroscopic data** 10
- **Emission spectroscopic data** 18
- **Lifetimes** 20

Quantum yields 22

- **(*E*)→(*Z*) photoisomerization process** 23
- **(*Z*)→(*E*) photoisomerization process** 29

NMR study of CIS-QDs and AzoAA interaction 30

Thermal back isomerisation 31

References 34

Determination of photoswitch loading on CIS-QDs surface

Table S1: Summary of the amount of **AzoDHLA** supplied during the synthesis and the average amount of photoswitch grafted on CIS-QDs surface after the purification process for each **CIS@n_Azo** batches.

	Volume of **AzoDHLA** solution added (µL)	Amount of **AzoDHLA** supplied in the synthesis (µmol)	Average number of photoswitchable units on the surface of CIS-QDs[a]
CIS@6_(*E*)-Azo	9.4	0.575	6
CIS@13_(*E*)-Azo	18.8	1.15	13
CIS@20_(*E*)-Azo	37.6	2.3	20
CIS@30_(*E*)-Azo	94	5.75	30
CIS@40_(*E*)-Azo	188	11.5	40
CIS@61_(*E*)-Azo	1880	115	61

[a]*Determined from UV/vis spectroscopic data by the Lambert-Beer law.*

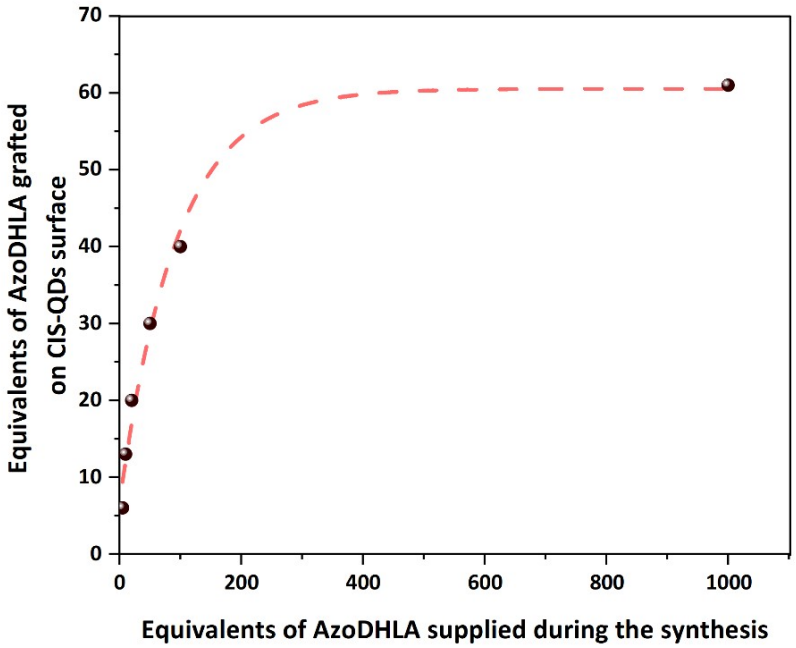

Figure S1: Correlation between the amount of **AzoDHLA** supplied during the synthesis and the amount of photoswitch grafted on the surface of CIS-QDs in **CIS@n_Azo** after purification.

NMR spectra

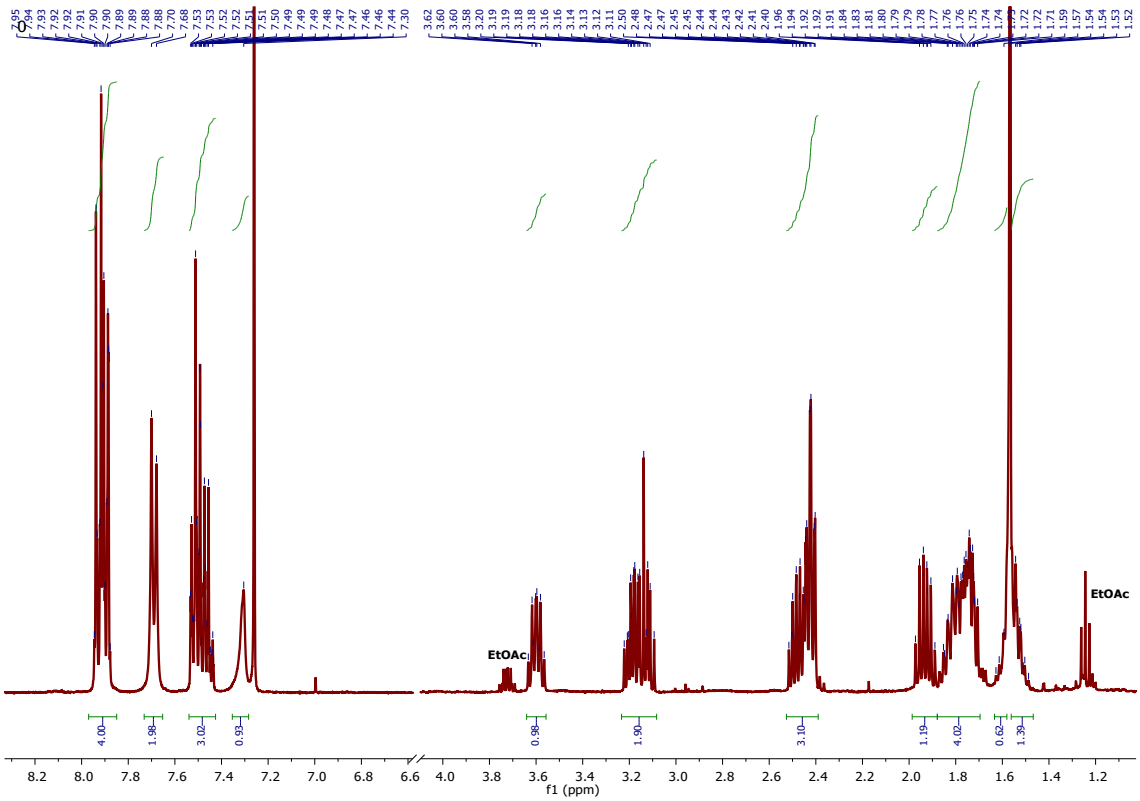

Figure S2: ^{1}H NMR spectrum of **(*E*)-AzoLA** ($CDCl_3$, 400 MHz).

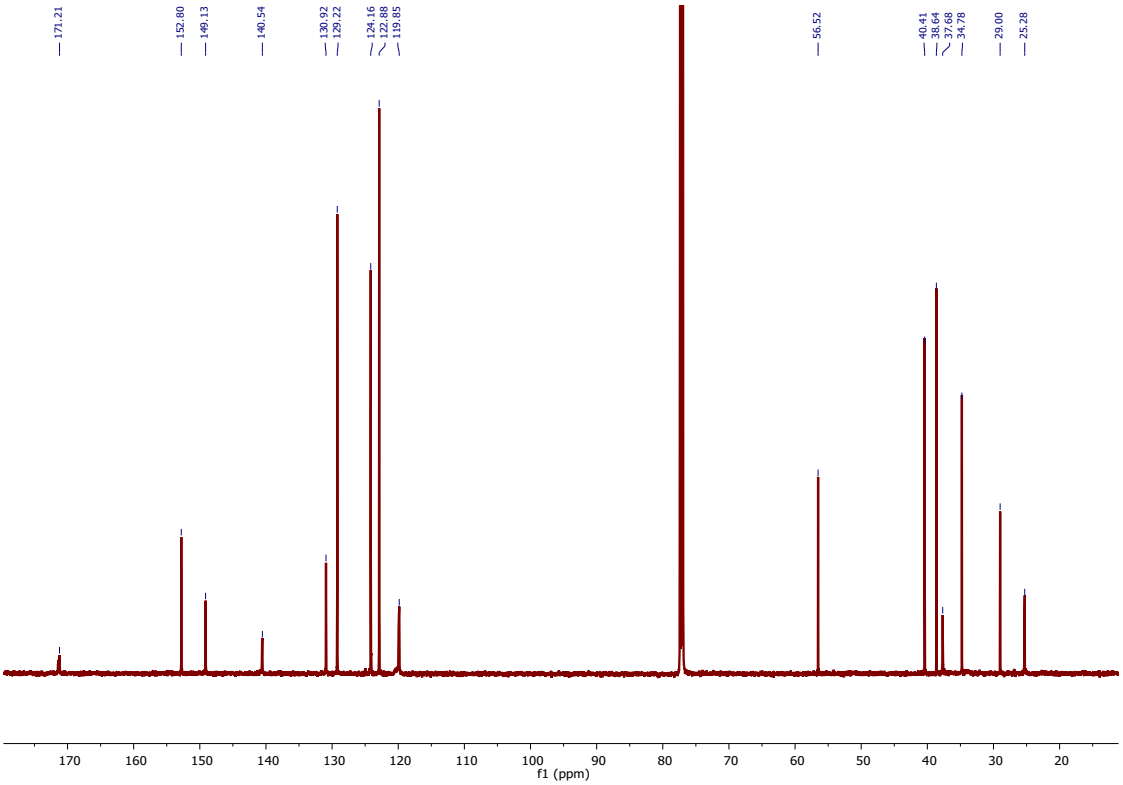

Figure S3 : $^{13}C\{^{1}H\}$ NMR spectrum of **(*E*)-AzoLA** ($CDCl_3$, 150 MHz).

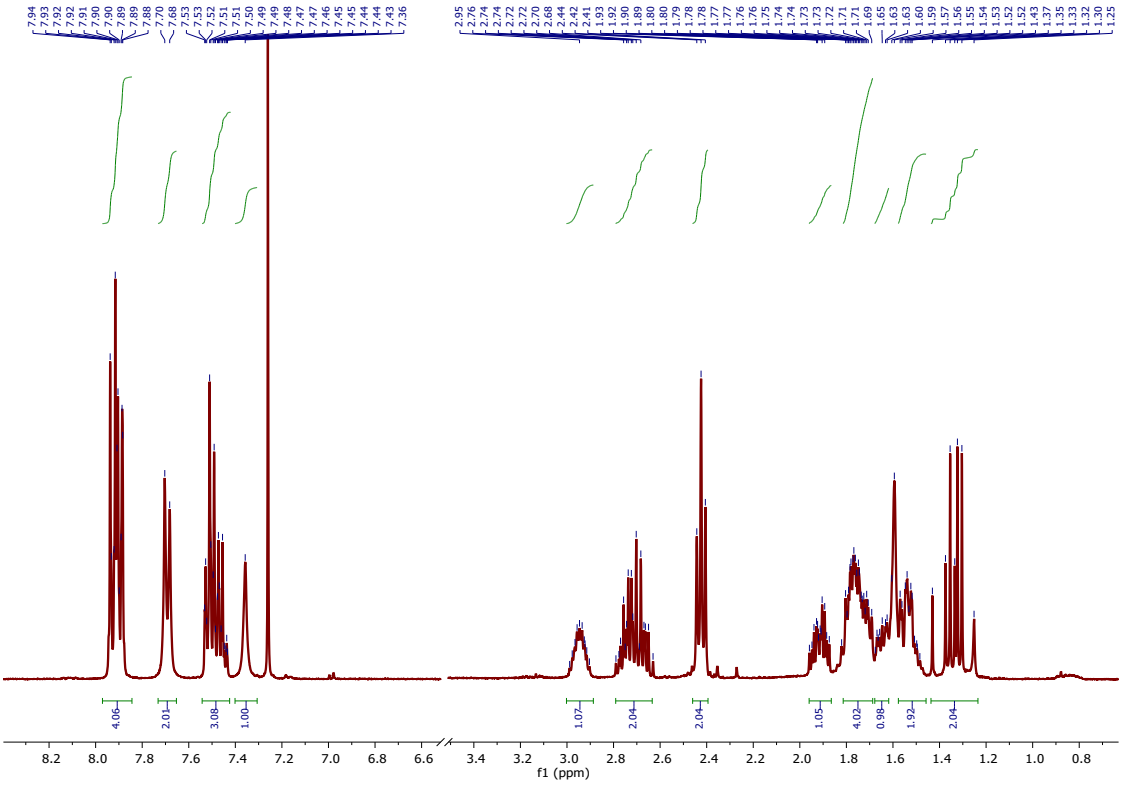

Figure S4: ^{1}H NMR spectrum of **(*E*)-AzoDHLA** ($CDCl_3$, 400 MHz).

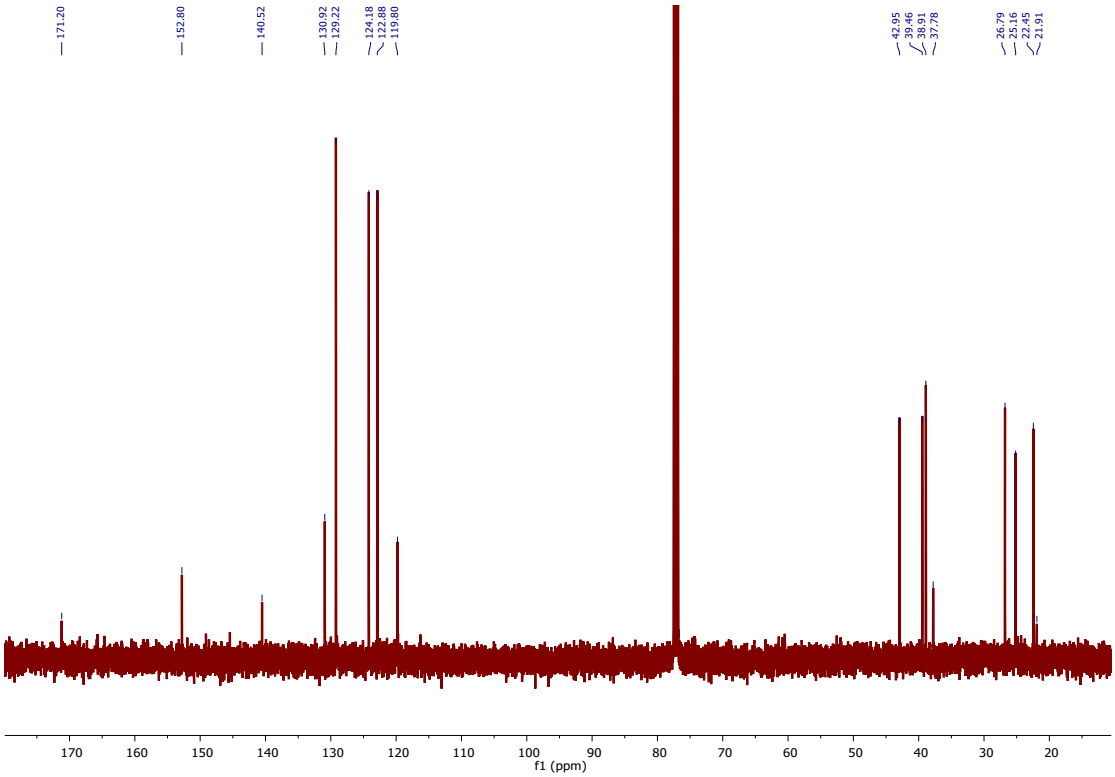

Figure S5: $^{13}C\{^{1}H\}$ NMR spectrum of **(*E*)-AzoDHLA** ($CDCl_3$, 100 MHz).

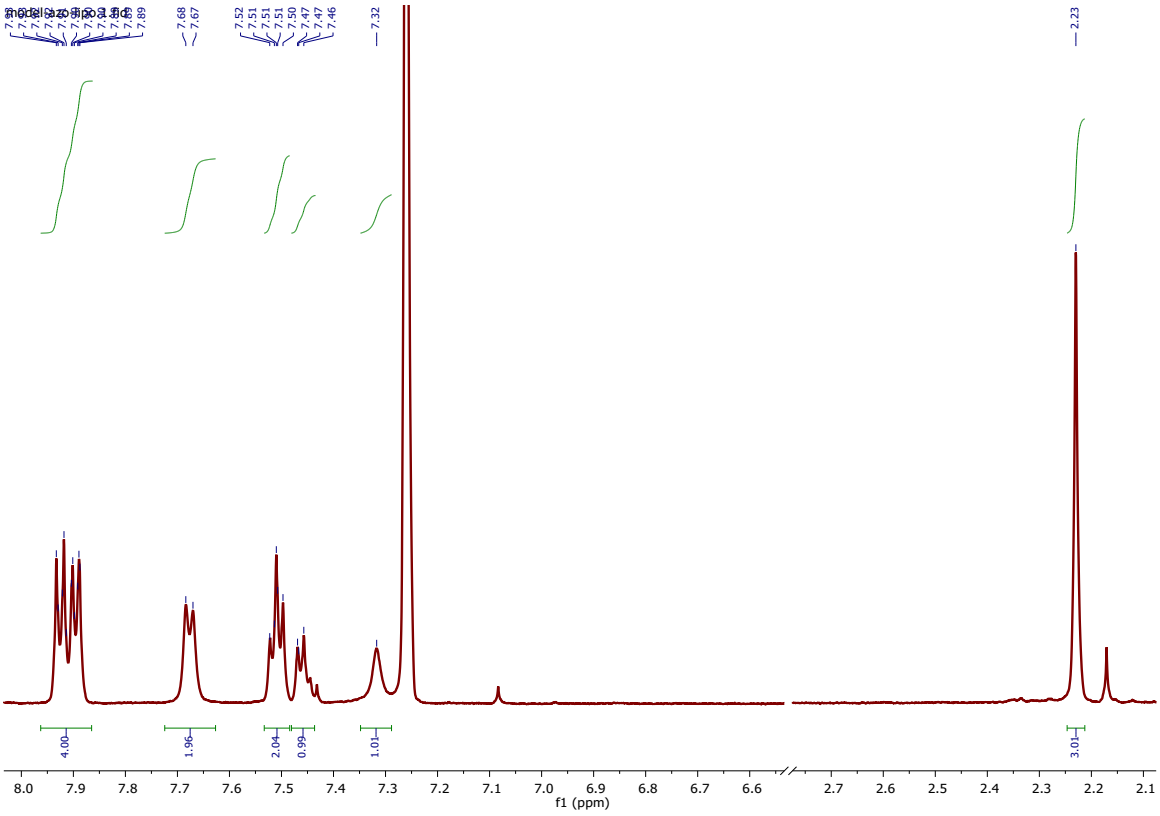

Figure S6: ^{1}H NMR spectrum of **(*E*)-AzoAA** ($CDCl_3$, 500 MHz).

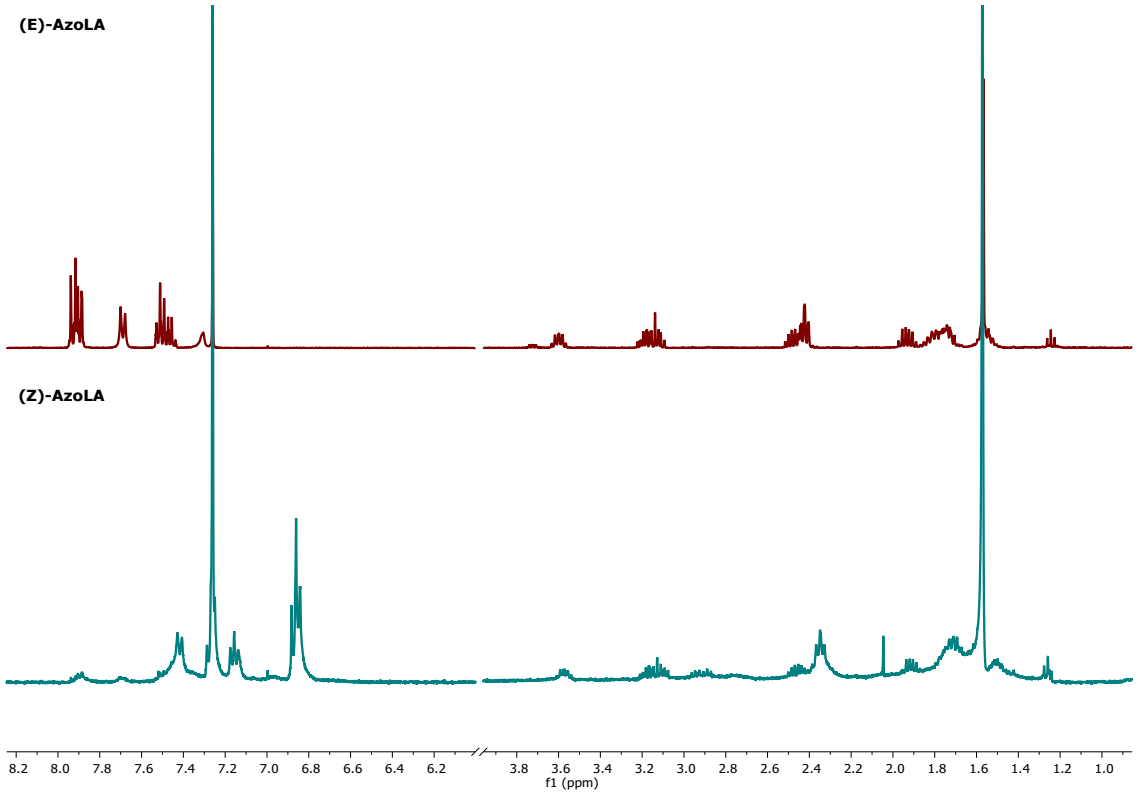

Figure S7: ^{1}H NMR spectrum of **(*E*)-AzoLA** before irradiation (top) and after irradiation at 365 nm (bottom) in ($CDCl_3$, 400 MHz).

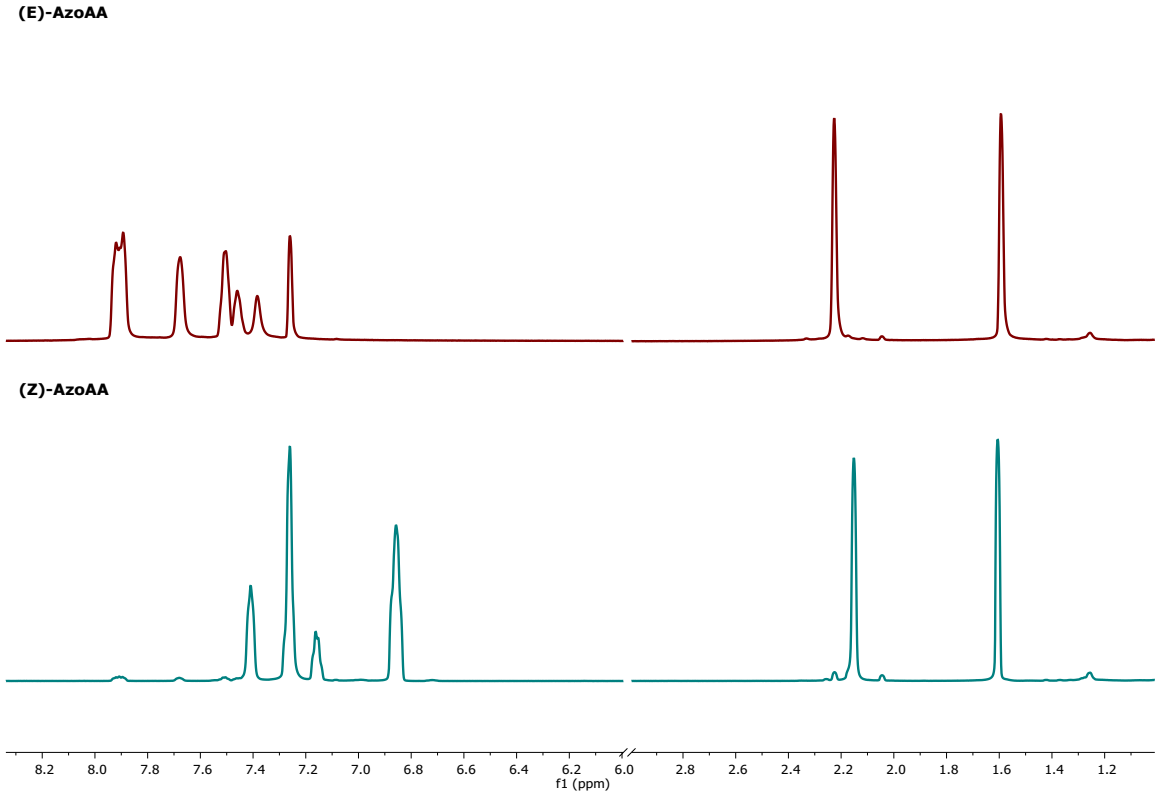

Figure S8 : ^{1}H NMR spectrum of **(*E*)-AzoAA** before irradiation (top) and after irradiation at 365 nm (bottom) ($CDCl_3$, 600 MHz).

(S)TEM Analysis

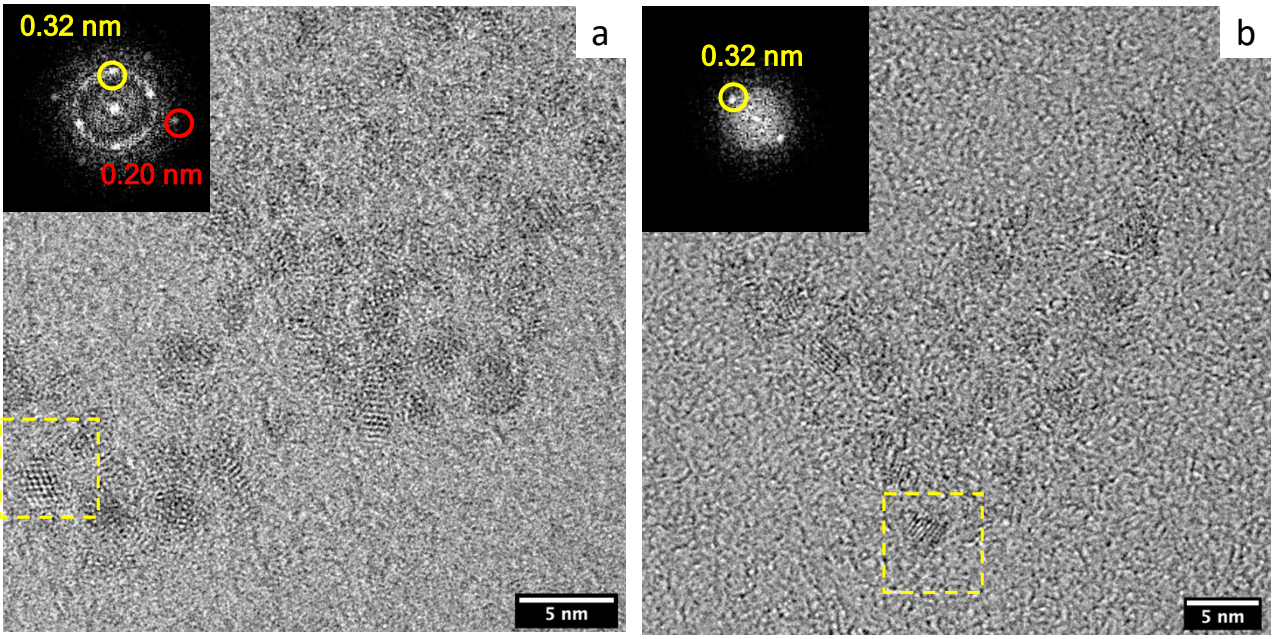

Figure S9: High resolution TEM micrographs of the **CIS-QDs**. Fourier transform in the inset (every FFT refers to a single particle, highlighted in the image by the square dotted in yellow).

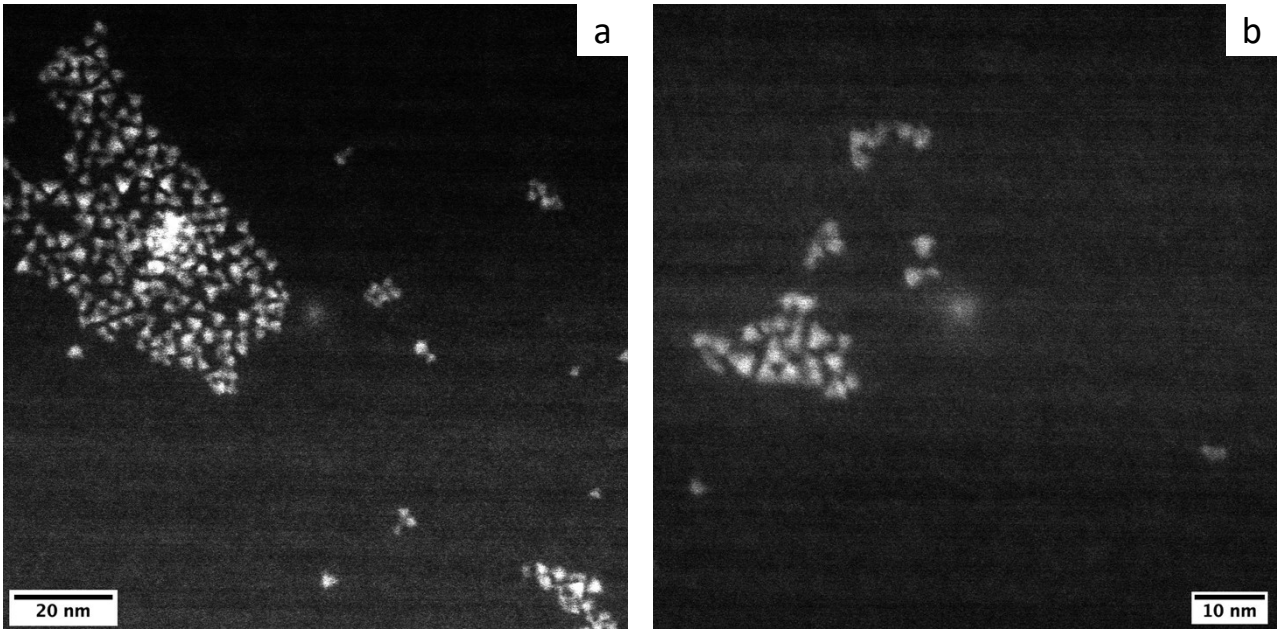

Figure S10: HAADF – STEM micrographs at different magnifications of the **CIS-QDs**.

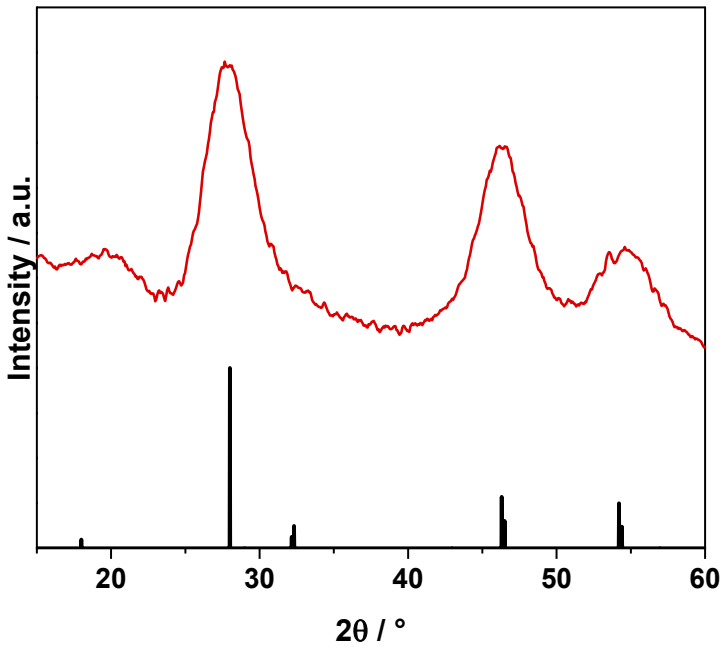

Figure S11: XRD pattern of **CIS-QDs** illustrating the characteristic planes of chalcopyrite phase of $CuInS_2$.

Absorption and emission spectroscopic data

Absorption spectroscopic data

The dimension of CIS-QDs, their molar absorption coefficient and the band gap of **CIS-QDs** and **CIS@*n*_Azo** were determined through the formulas reported by Booth et. *al.*[1]

The dimension was calculated as follows:

$$d = 68.952 - 0.2136\,\lambda_{PL} + 1.717 \times 10^{-4}\,\lambda_{PL}{}^{2} = 4.1\ nm$$

Where λ_{PL} is the maximum of the emission band of **CIS-QDs** capped with octanethiol.

ε_{CIS} at 400 nm (3.1 eV) was calculated by the following formula:

$$\varepsilon_{CIS}\,(400\ nm) = 2123 \times d^{3.8} = 4.40 \times 10^{5}\,M^{-1}cm^{-1}$$

where d is the dimension of the CIS core, which in our case is 4.1 nm according to the previously reported formula.

The band gap of pristine **CIS-QDs** as well as those of **CIS@n_Azo** were determined by localizing the local minimum of the second derivative of the absorption spectra of **CIS-QDs** and **CIS@n_Azo** in the range 400-600nm.

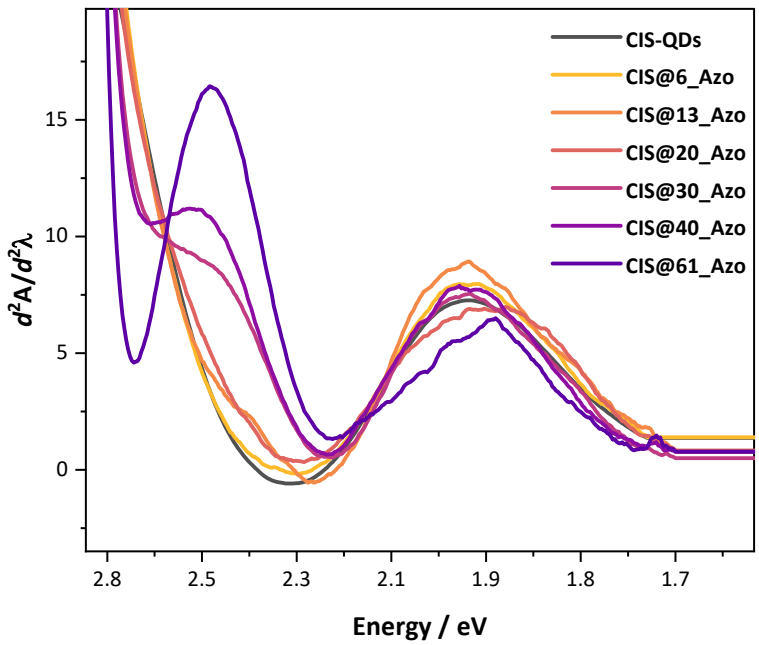

Figure S12: Second derivative of the absorption spectra of **CIS-QDs** and **CIS@n_(*E*)-Azo**

The concentration of **CIS-QDs** stock solution was determined by the Lambert-Beer law, using the molar absorption coefficient calculated as reported previously.

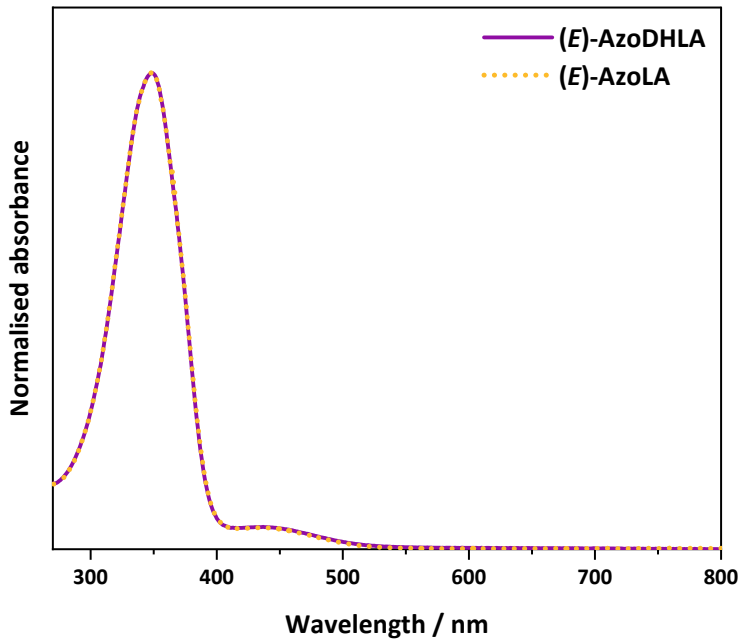

Figure S13: Comparison of absorption spectra of **(*E*)-AzoDHLA** (purple solid line) and **(*E*)-AzoLA** (blue dot line) in chloroform.

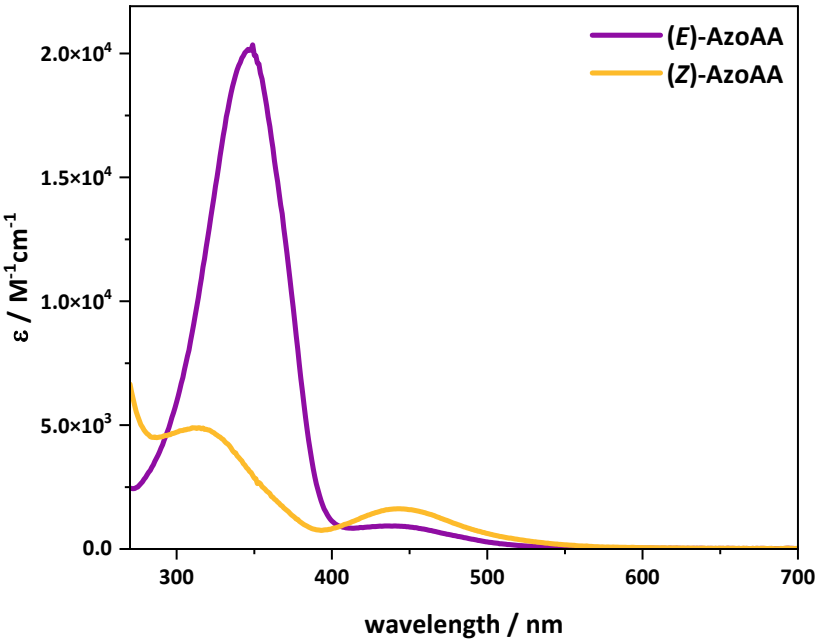

Figure S14: Absorption spectra of **(*E*)-AzoAA** (purple line) and **(*Z*)-AzoAA** (yellow line) in chloroform.

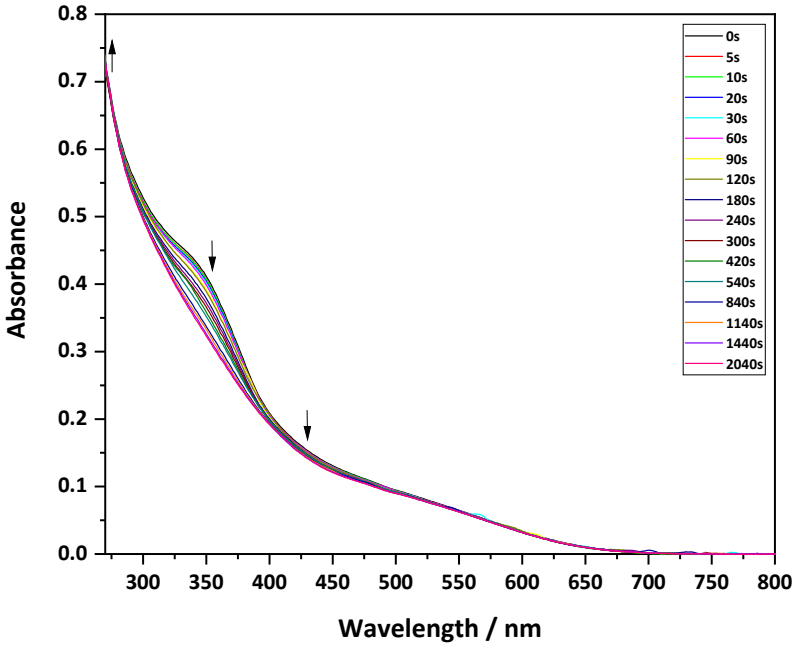

Figure S15: UV-Vis absorption spectra evolution of a solution of **CIS@6_(*E*)-Azo** in chloroform (~5x10^{-7} M) during irradiation at λ_{ex} = 365 nm.

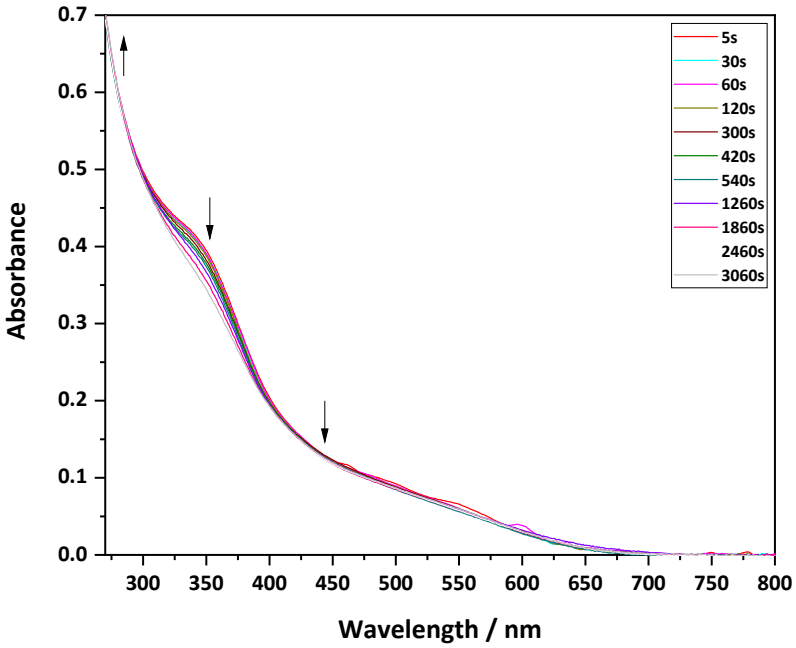

Figure S16: UV-Vis absorption spectra evolution of a solution of **CIS@6_(*E*)-Azo** in chloroform (~5x10^{-7} M) during irradiation at λ_{ex} = 436 nm.

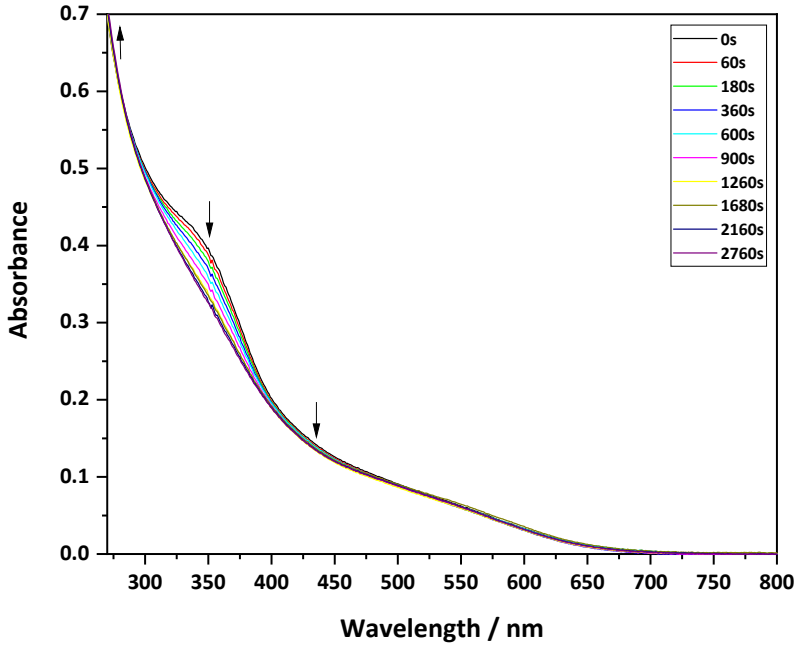

Figure S17: UV-Vis absorption spectra evolution of a solution of **CIS@6_(*E*)-Azo** in chloroform (~5x10^{-7} M) during irradiation at λ_{ex} = 533 nm.

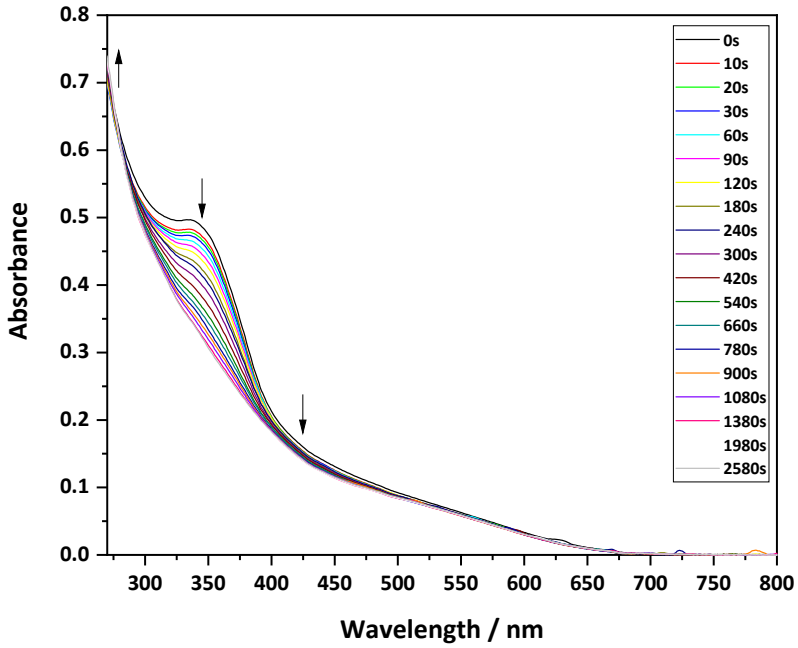

Figure S18 : UV-Vis absorption spectra evolution of a solution of **CIS@13_(*E*)-Azo** in chloroform (~5x10^{-7} M) during irradiation at λ_{ex} = 365 nm.

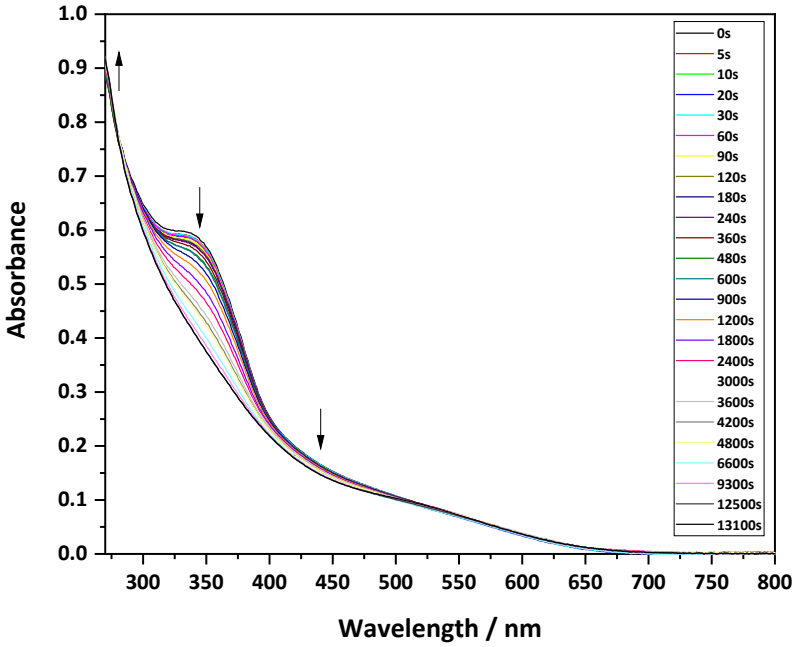

Figure S19: UV-Vis absorption spectra evolution of a solution of **CIS@13_(*E*)-Azo** in chloroform (~5x10^{-7} M) during irradiation at λ_{ex} = 436 nm.

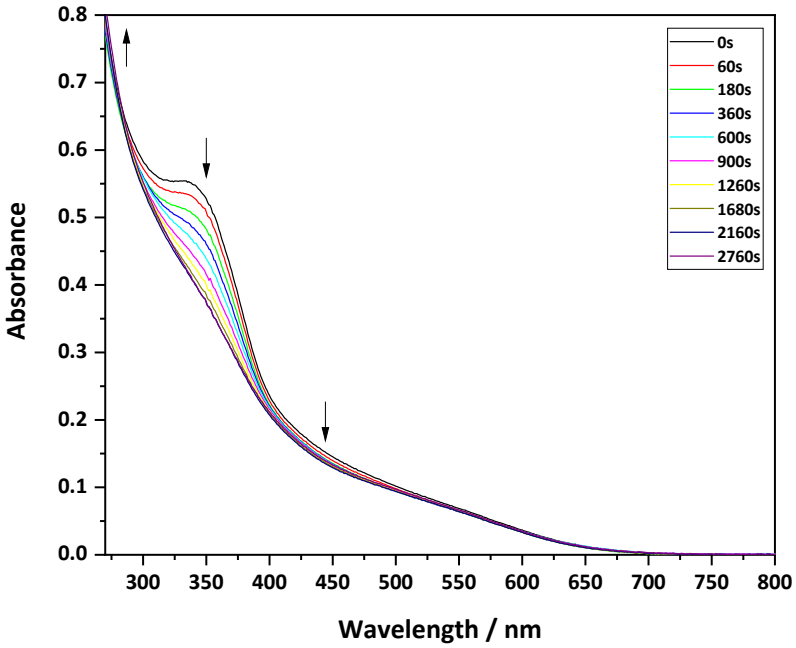

Figure S20: UV-Vis absorption spectra evolution of a solution of **CIS@13_(*E*)-Azo** in chloroform (~5x10^{-7} M) during irradiation at λ_{ex} = 533 nm.

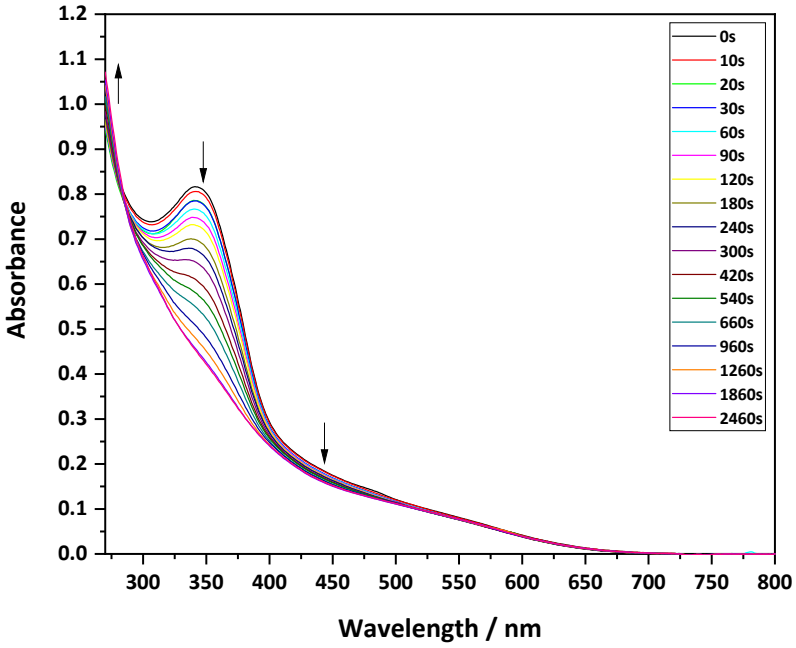

Figure S21: UV-Vis absorption spectra evolution of a solution of **CIS@20_(*E*)-Azo** in chloroform (~5x10^{-7} M) during irradiation at λ_{ex} = 365 nm.

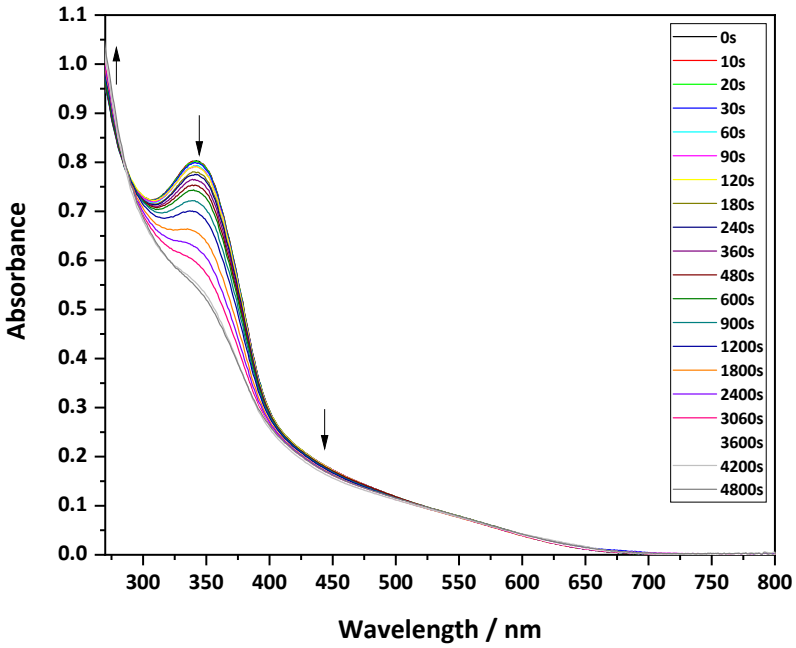

Figure S22: UV-Vis absorption spectra evolution of a solution of **CIS@20_(*E*)-Azo** in chloroform (~5x10^{-7} M) during irradiation at λ_{ex} = 436 nm.

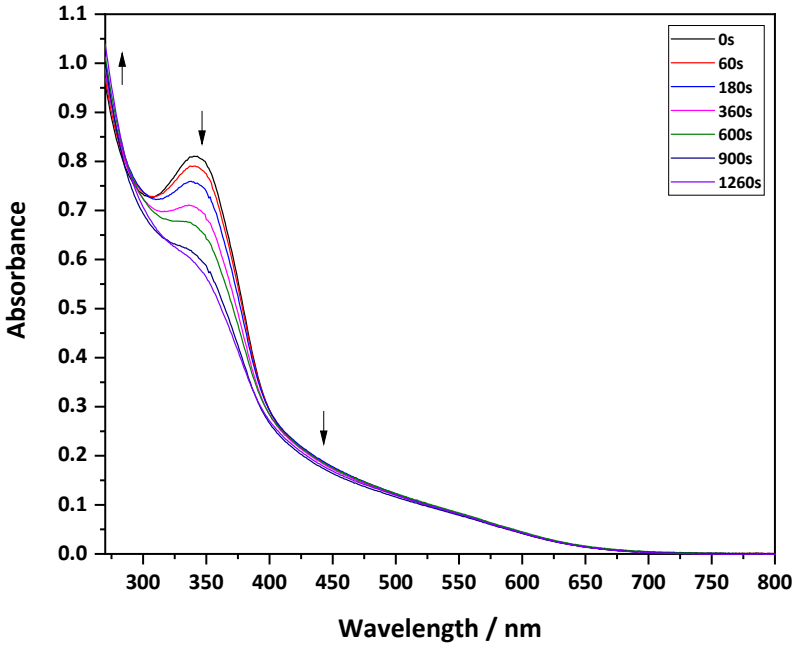

Figure S23: UV-Vis absorption spectra evolution of a solution of **CIS@20_(*E*)-Azo** in chloroform (~5x10^{-7} M) during irradiation at λ_{ex} = 533 nm.

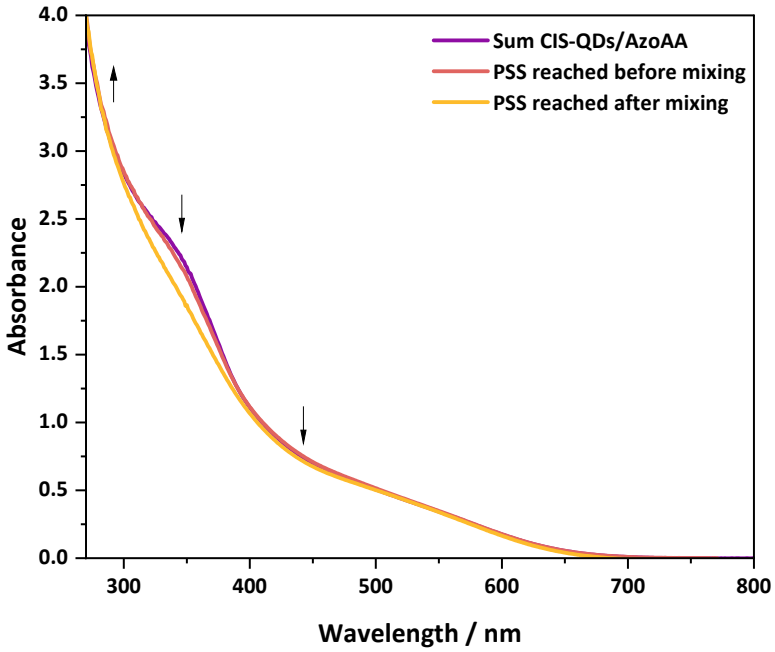

Figure S24: Absorption spectra of solutions of **CIS-QDs** (1.15x10^{-6} M) and **(*E*)-AzoAA** (5.0x10^{-5} M) in chloroform, recorded in a two-chamber Yankeelov cuvette. Before mixing and irradiation at 533 nm (purple), before mixing and after irradiation at 533 nm to reach PSS (red) and after mixing and further irradiation at 533 nm to achieve PSS (yellow).

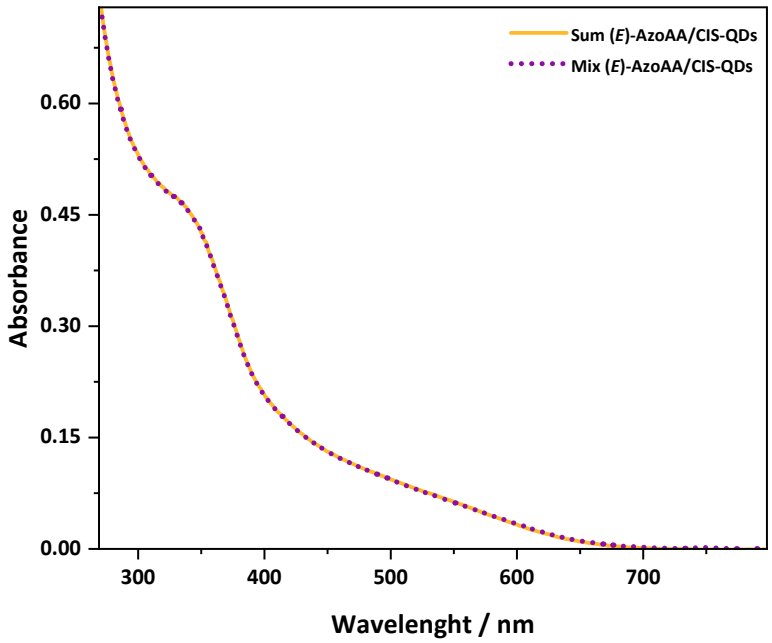

Figure S25: Absorption spectra of **CIS-QDs** ($1x10^{-6}$ M) and **(*E*)-AzoAA** ($1x10^{-5}$ M) in chloroform, recorded in a two-chamber cuvette before (yellow) and after mixing (purple).

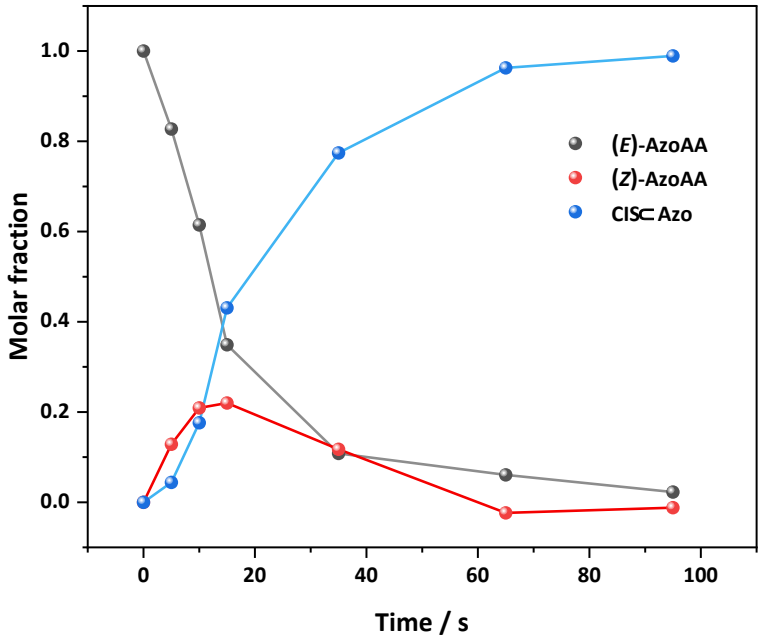

Figure S26: Evolution of the composition of a solution of **CIS-QDs** ($1x10^{-6}$ M) and **(*E*)-AzoAA** ($5x10^{-5}$ M) under irradiation at 365 nm. Molar fraction of **(*E*)-AzoAA** (grey), **(*Z*)-AzoAA** (red) and **CIS⊂(*Z*)-AzoAA** (blue)

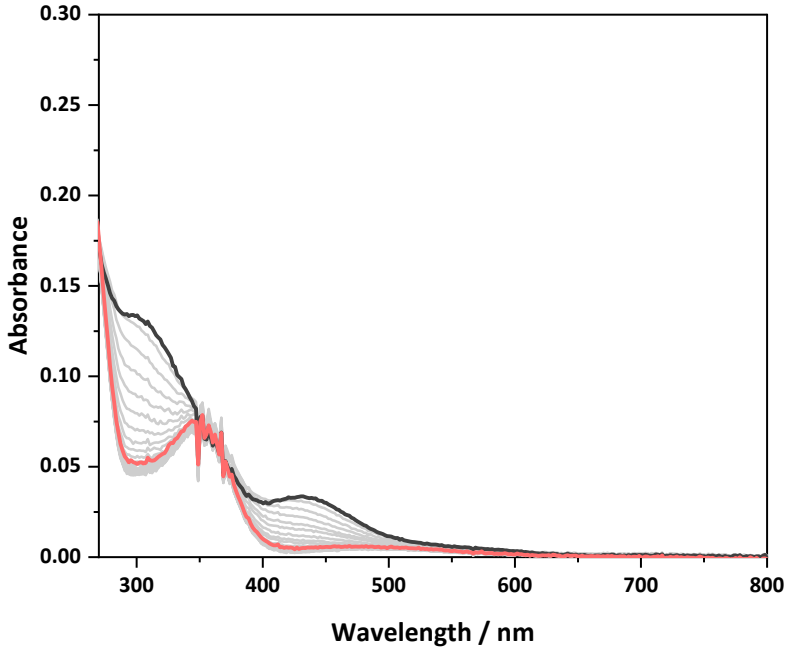

Figure S27: UV-Vis absorption spectra evolution of a solution of 6% **(*E*)-AzoAA** and 94% **(*Z*)-AzoAA** (PSS reached under 365 nm irradiation, initial concentration of **(*E*)-AzoAA** is $5x10^{-5}$ M) in chloroform kept in dark under stirring after mixing with a solution of **CIS-QDs** ($1x10^{-6}$ M). Reference is a solution of **CIS-QDs** ($1x10^{-6}$ M).

Emission spectroscopic data

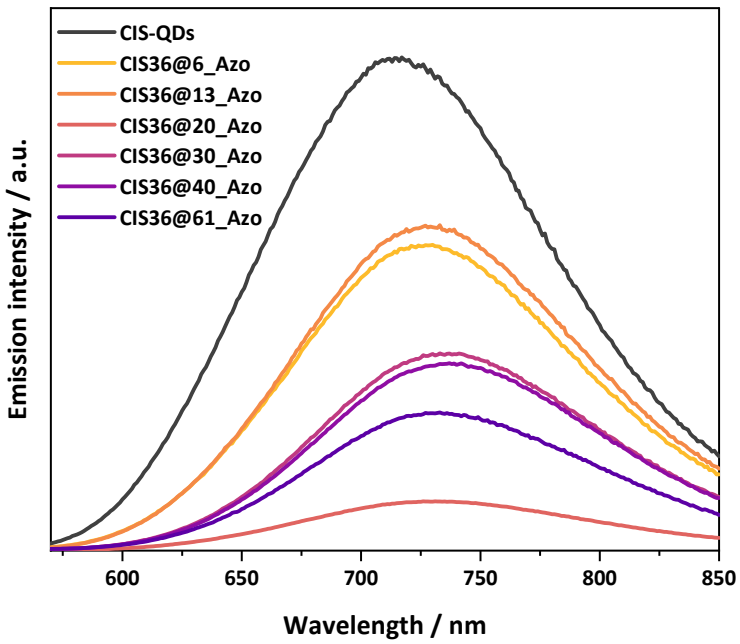

Figure S28: Emission spectra of **CIS-QDs** and **CIS@n_(*E*)-Azo**, scaled on their PLQY (λ_{exc} : 548 nm).

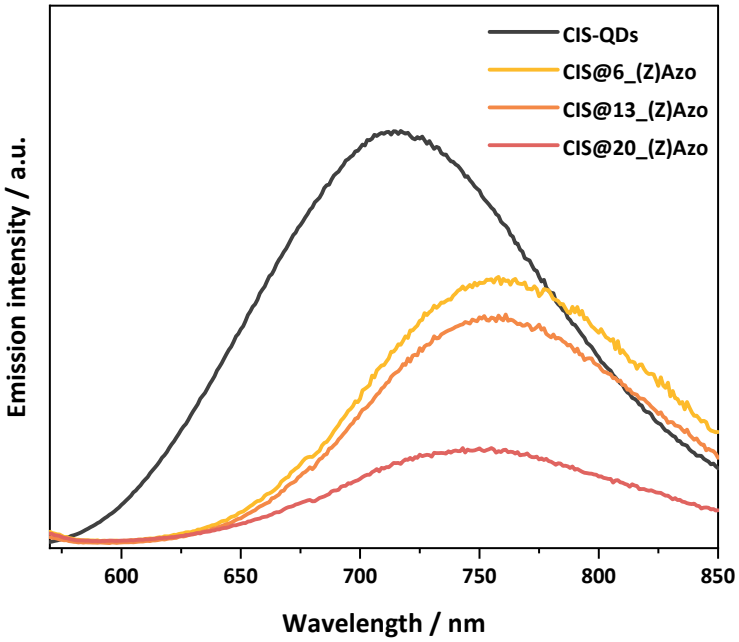

Figure S29: Emission spectra of **CIS-QDs** and **CIS@n_(*Z*)-Azo**, scaled on their PLQY (λ_{exc} : 548 nm).

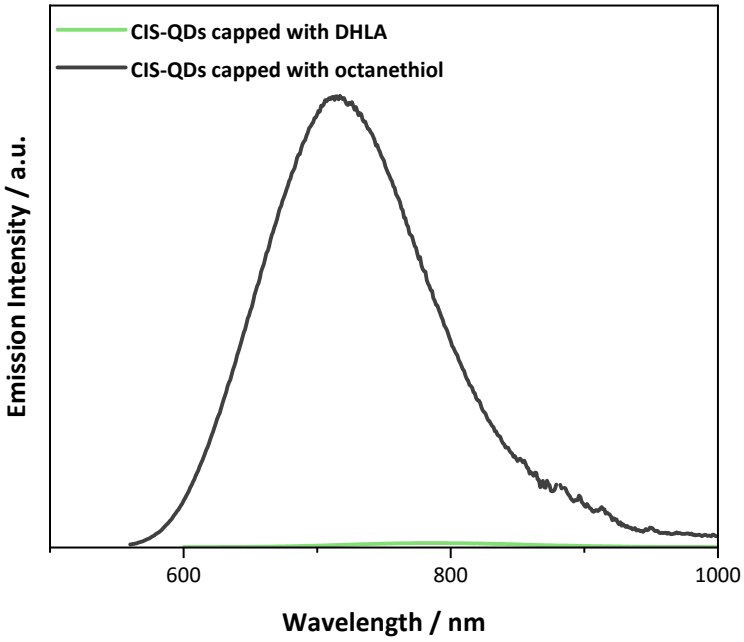

Figure S30 : Emission spectra of pristine **CIS-QDs** and **CIS-QDs** capped with **DHLA** after ligand exchange, scaled on their PLQY (λ_{exc} : 548 nm).

Table S2: Main photophysical properties of the **CIS-QDs/(*Z*)-AzoDHLA** hybrids in air-equilibrated chloroform solutions.

Sample	λ_{em} / nm	FWHM / nm	PLQY[a] / %	τ_1 / ns	τ_2/ ns	τ_{ave}[b] / ns
CIS-QDs	717	134	12	87	352	219
CIS@6_(*Z*)-AZO	730	128	6	67	324	141
CIS@13_(*Z*)-AZO	733	128	6	60	288	121
CIS@20_(*Z*)-AZO	731	127	2	51	250	87
CIS@30_(*Z*)-AZO	733	123	N.D.	N.D.	N.D.	N.D.
CIS@40_(*Z*)-AZO	737	123	N.D.	N.D.	N.D.	N.D.
CIS@61_(*Z*)-AZO	732	124	N.D.	N.D.	N.D.	N.D.
AzoLA	-[c]	-[c]	-[c]	-[c]	-[c]	-[c]

[a]Excitation at 548 nm. Determined by actinometry. [b]Weighted averaged lifetime, excitation at 405 nm. Emission detection at 730 nm. [c]No emission detected. N.D. Non determined.

Lifetimes

All the emission decays were fitted by a biexponential function, yielding two lifetimes (τ_1 and τ_2) with the corresponding pre-exponential factors (B_1 and B_2) The average lifetimes of all samples were determined by the following formula:

$$\tau_{ave} = \frac{\tau_1 \times B_1 + \tau_2 \times B_2}{B_1 + B_2}$$

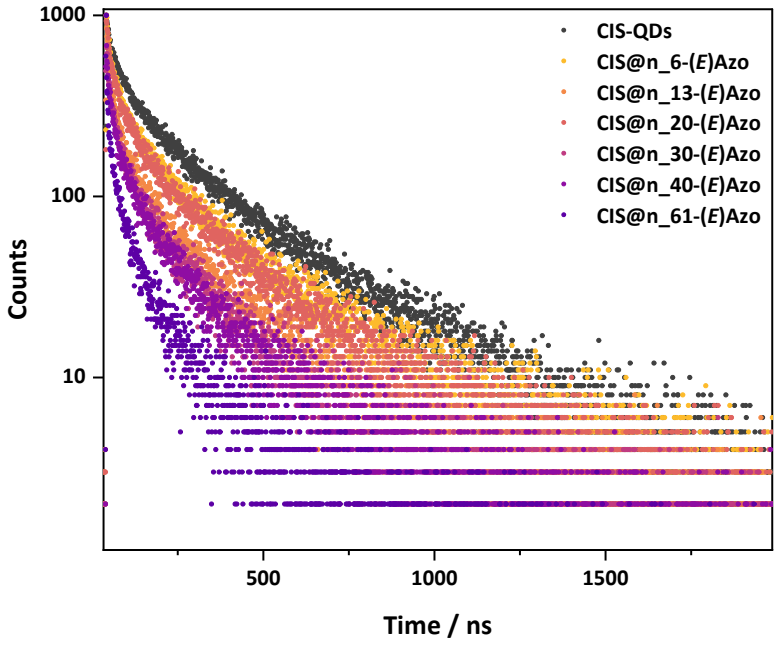

Figure S31 : Emission decays of **CIS-QDs** (black dots) and **CIS@n_(*E*)Azo** (colored dots). λ_{exc} : 548 nm; detected λ_{em} : 730 nm.

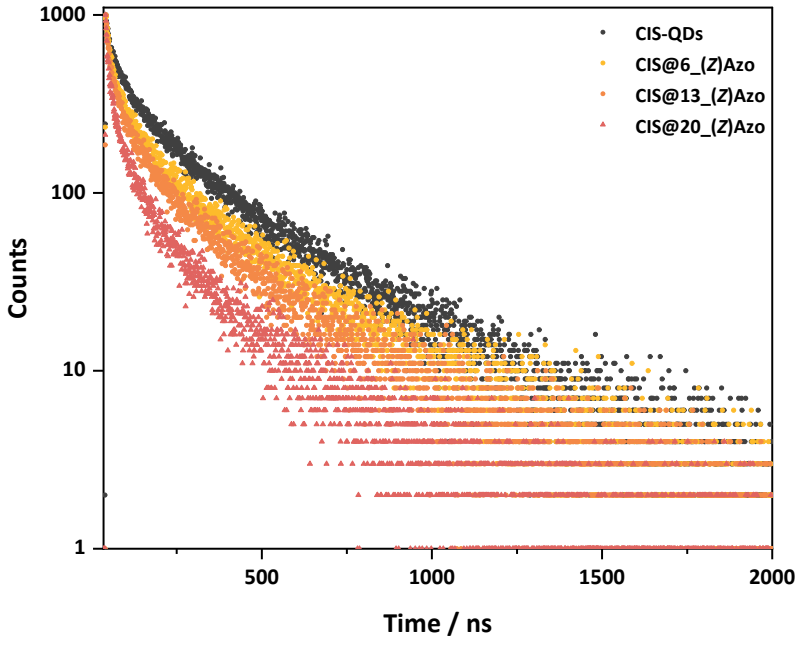

Figure S32 : Emission decays of **CIS-QDs** (black dots) and **CIS@n_(*Z*)Azo** (colored dots). λ_{exc} : 548 nm; detected λ_{em} : 730 nm.

Quantum yields

Quantum yields for the photoinduced ring-opening process ($\phi_{(E)\rightarrow(Z)}$ and $\phi_{(Z)\rightarrow(E)}$) were determined by illumination of solutions of (*E*) and (*Z*) isomers at room temperature using monochromatic light. Samples were placed at 5 cm from the irradiation source. The photon flux was determined using ferrioxalate actinometer. Quantum yields were then determined by fitting the results using the photo-kinetic model reported by Maafi and Brown[2,3] using the following equation:

$$Abs_{tot}^{\lambda_{obs}}(t) = \varepsilon_{(Z)}^{\lambda_{obs}} C_0 l_{probe} + \frac{\varepsilon_{(E)}^{\lambda_{obs}} - \varepsilon_{(Z)}^{\lambda_{obs}}}{\varepsilon_{(E)}^{\lambda_{irr}}} \left(\frac{l_{probe}}{l_{irr}}\right) \times \log\left[1 + \left(10^{\varepsilon_{(E)}^{\lambda_{obs}} l_{irr} C_{(E)}(0)} - 1\right) \times e^{-\left(\phi_{(E)\rightarrow(Z)}^{\lambda_{irr}} \varepsilon\right.}\right.$$

where in this formula:

- $Abs_{tot}^{\lambda_{obs}}(t)$: Total absorbance of the system at observation wavelength
- C_0: Concentration of the sample at t=0
- $C_{(E)}(0)$: Concentration of (*E*) isomer at t=0
- l_{probe}: Observation optical path length
- l_{irr}: Irradiation optical path length
- $\phi_{(E)\rightarrow(Z)}^{\lambda_{irr}}$: (*E*)→(*Z*) isomerization quantum yield
- $\varepsilon_{(E)}^{\lambda_{obs}}$: Molar extinction coefficients of (*E*) isomer at observation wavelength
- $\varepsilon_{(Z)}^{\lambda_{obs}}$: Molar extinction coefficients of (*Z*) isomer at observation wavelength
- $\varepsilon_{(E)}^{\lambda_{irr}}$: Molar extinction coefficients of (*E*) isomer at irradiation wavelength
- $I_0^{\lambda_{irr}}$: Irradiation power received by the sample

From a practical point of view, the evolution of the absorption was monitored by UV-Visible spectroscopy over time and the absorbance was plotted as a function of time. From the recorded absorption profiles, a Levenberg-Marquardt iterative program within the Origin 9.5.0 software package was used for the determination of the best fit curves.

(*E*)→(*Z*) photoisomerization process

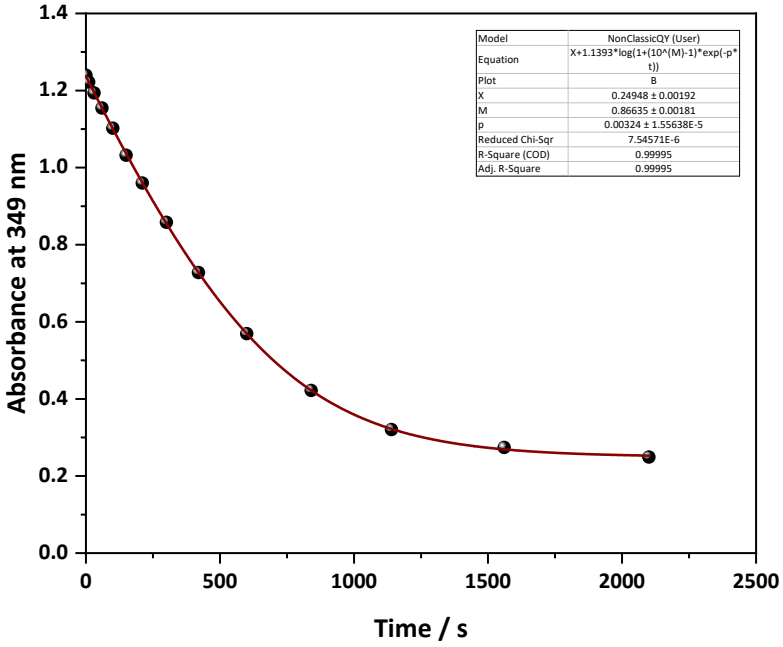

Figure S33: Evolution of the absorbance at λ = 349 nm during irradiation at λ_{ex} = 365 nm of **(*E*)-AzoLA** in chloroform as function of time and corresponding fit using Maafi and Brown photo-kinetic model.[2,3]

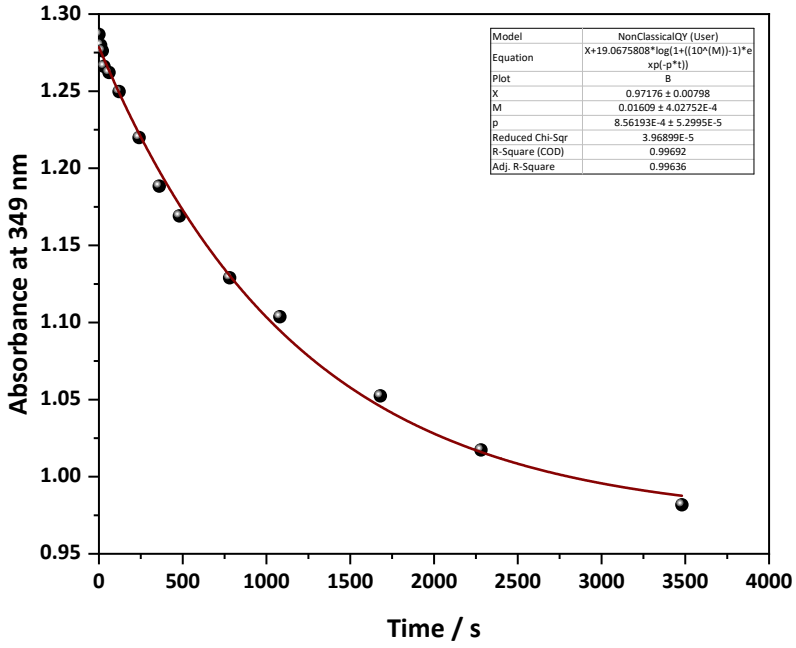

Figure S34: Evolution of the absorbance at λ = 349 nm during irradiation at λ_{ex} = 436 nm of **(*E*)-AzoLA** in chloroform as function of time and corresponding fit using Maafi and Brown[2,3] photo-kinetic model.

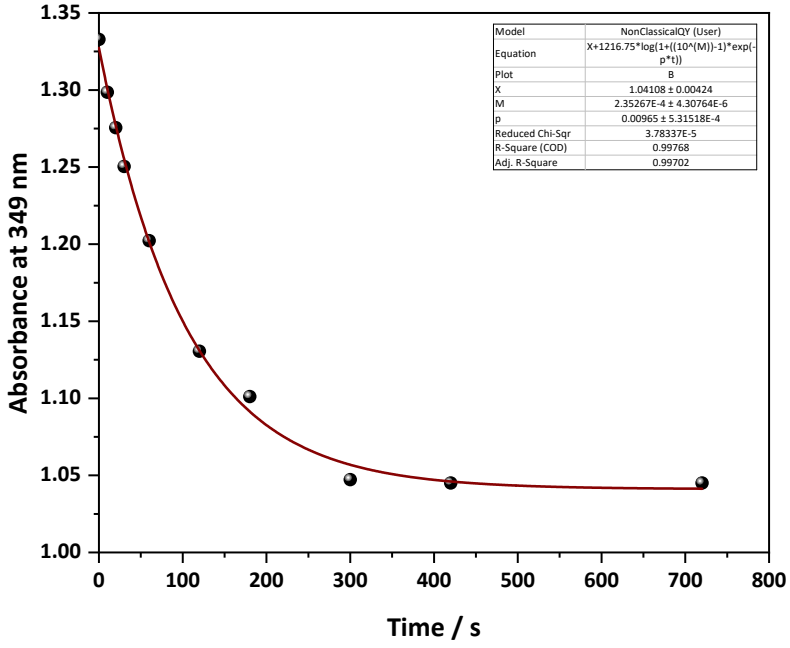

Figure S35: Evolution of the absorbance at λ = 349 nm during irradiation at λ_{ex} = 533 nm of **(*E*)-AzoLA** in chloroform as function of time and corresponding fit using Maafi and Brown[2,3] photo-kinetic model.

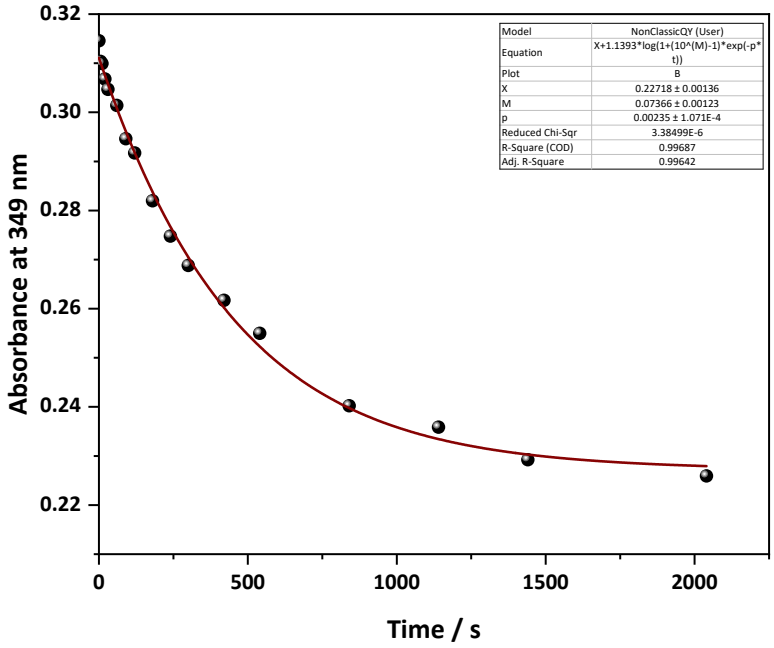

Figure S36: Evolution of the absorbance at λ = 349 nm during irradiation at λ_{ex} = 365 nm of **CIS@6_(*E*)-Azo** in chloroform as function of time and corresponding fit using Maafi and Brown[2,3] photo-kinetic model.

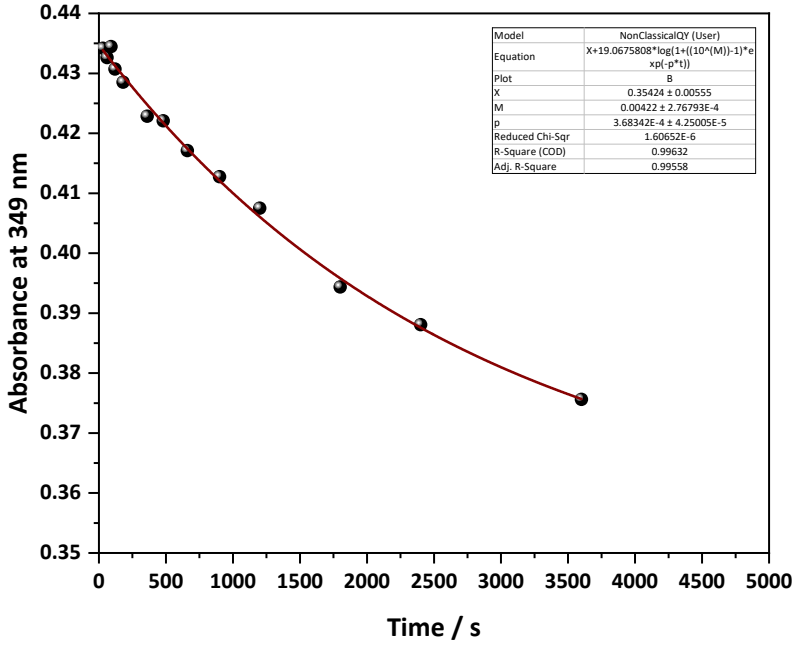

Figure S37: Evolution of the absorbance at λ = 349 nm during irradiation at λ_{ex} = 436 nm of **CIS@6_(*E*)-Azo** in chloroform as function of time and corresponding fit using Maafi and Brown[2,3] photo-kinetic model.

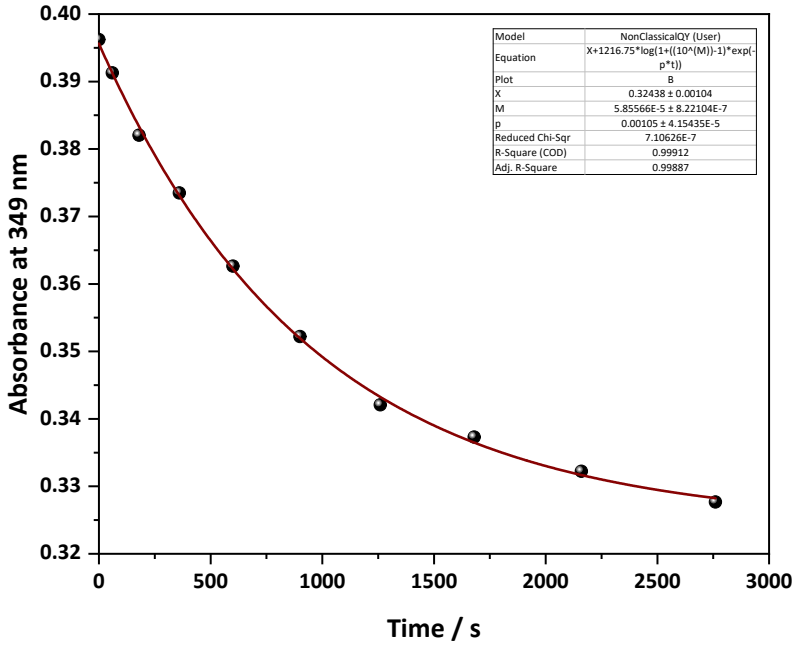

Figure S38: Evolution of the absorbance at λ = 349 nm during irradiation at λ_{ex} = 533 nm of **CIS@6_(*E*)-Azo** in chloroform as function of time and corresponding fit using Maafi and Brown[2,3] photo-kinetic model.

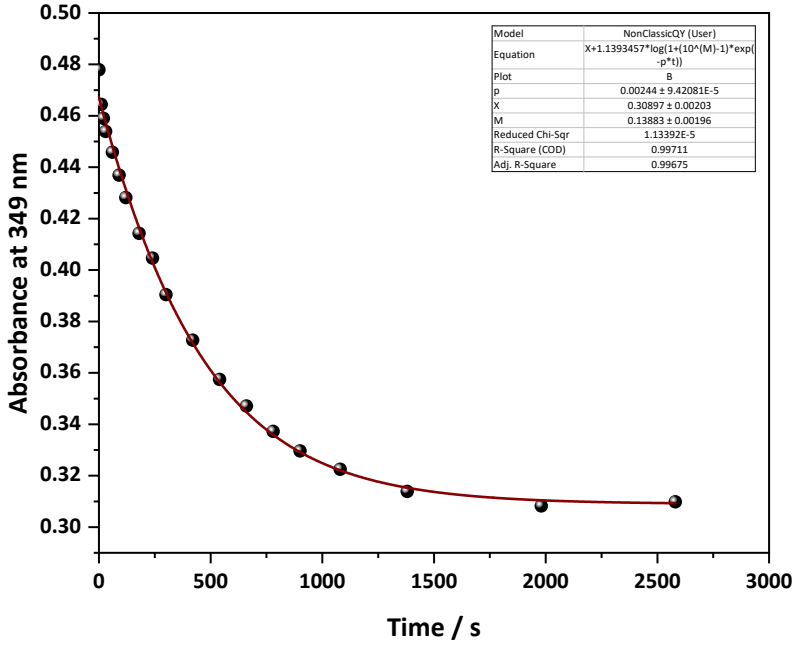

Figure S39: Evolution of the absorbance at λ = 349 nm during irradiation at λ_{ex} = 365 nm of **CIS@13_(*E*)-Azo** in chloroform as function of time and corresponding fit using Maafi and Brown[2,3] photo-kinetic model.

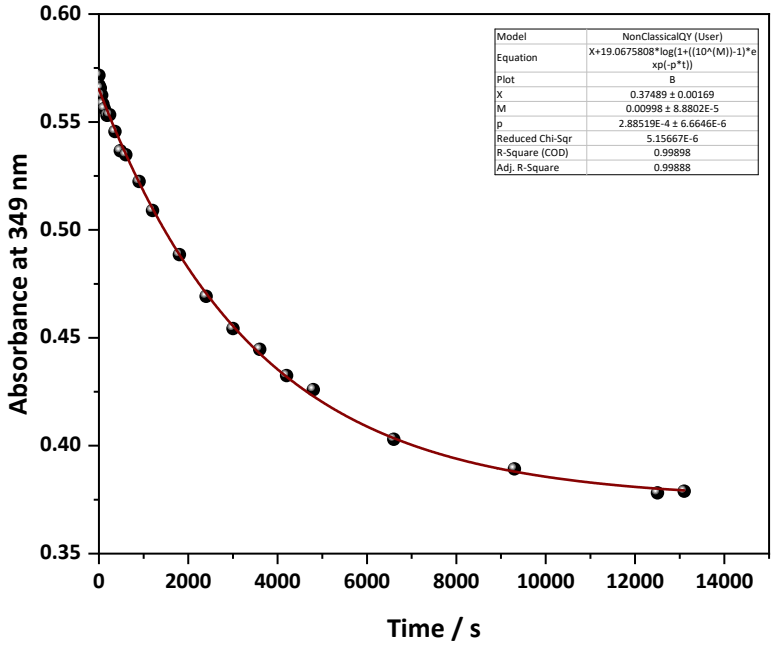

Figure S40: Evolution of the absorbance at λ = 349 nm during irradiation at λ_{ex} = 436 nm of **CIS@13_(*E*)-Azo** in chloroform as function of time and corresponding fit using Maafi and Brown[2,3] photo-kinetic model.

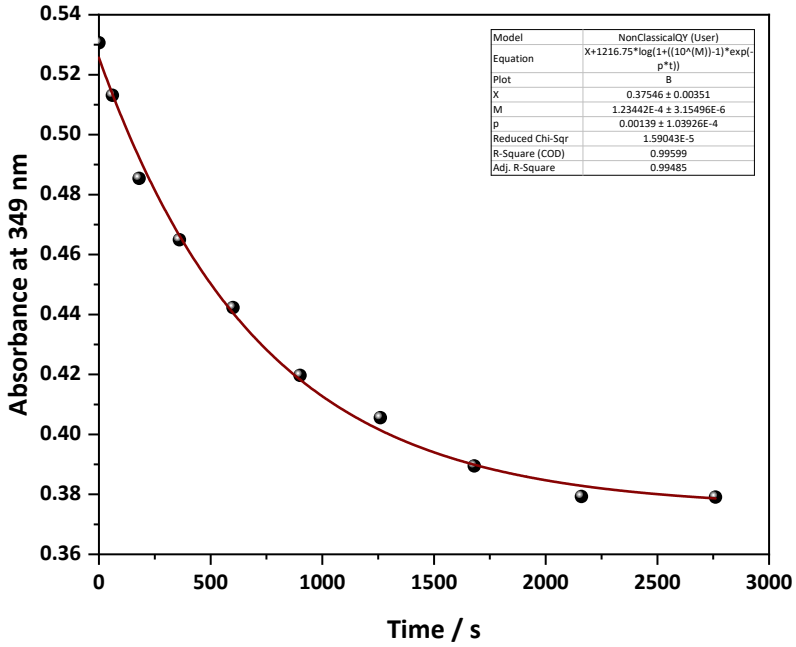

Figure S41: Evolution of the absorbance at λ = 349 nm during irradiation at λ_{ex} = 533 nm of **CIS@13_(*E*)-Azo** in chloroform as function of time and corresponding fit using Maafi and Brown[2,3] photo-kinetic model.

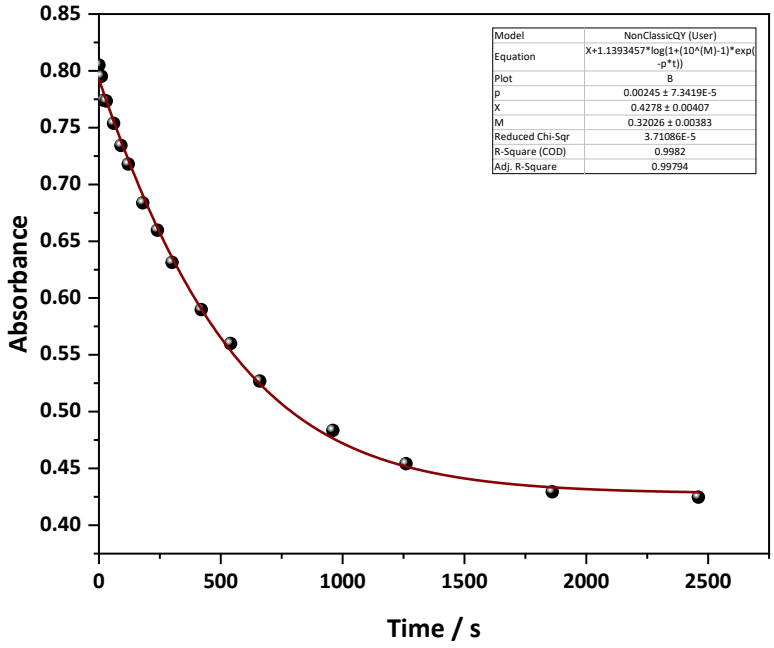

Figure S42: Evolution of the absorbance at λ = 349 nm during irradiation at λ_{ex} = 365 nm of **CIS@20_(*E*)-Azo** in chloroform as function of time and corresponding fit using Maafi and Brown[2,3] photo-kinetic model.

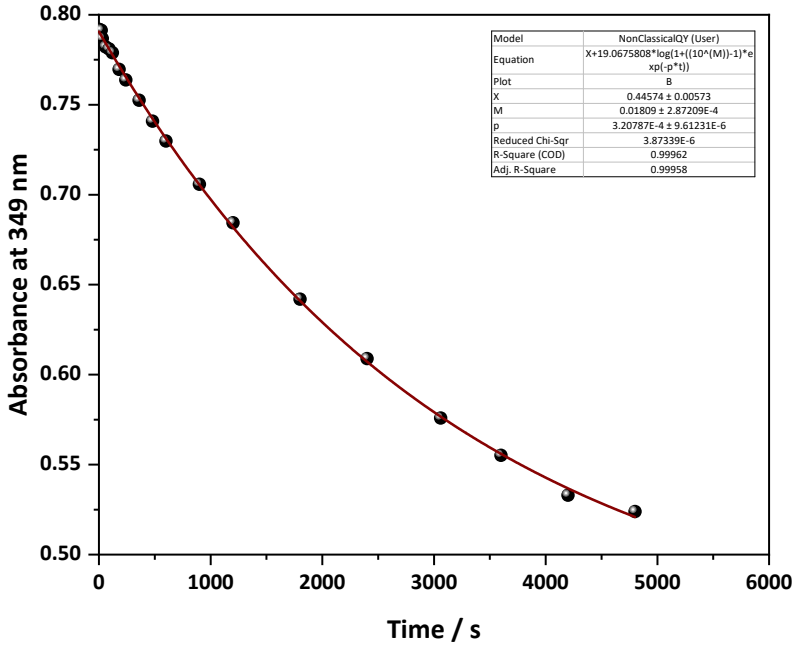

Figure S43: Evolution of the absorbance at λ = 349 nm during irradiation at λ_{ex} = 436 nm of **CIS@20_(*E*)-Azo** in chloroform as function of time and corresponding fit using Maafi and Brown[2,3] photo-kinetic model.

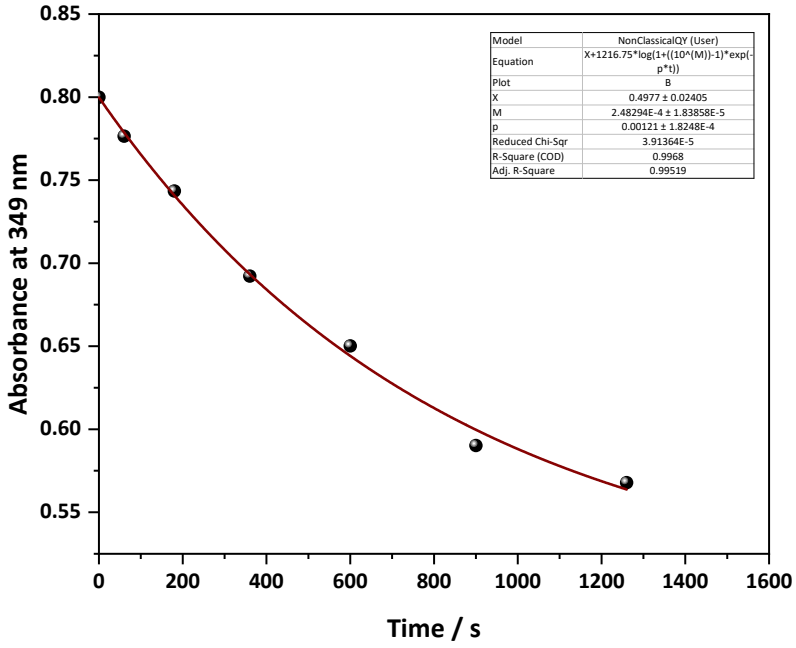

Figure S44: Evolution of the absorbance at λ = 349 nm during irradiation at λ_{ex} = 533 nm of **CIS@20_(*E*)-Azo** in chloroform as function of time and corresponding fit using Maafi and Brown[2,3] photo-kinetic model.

(*Z*)→(*E*) photoisomerization process

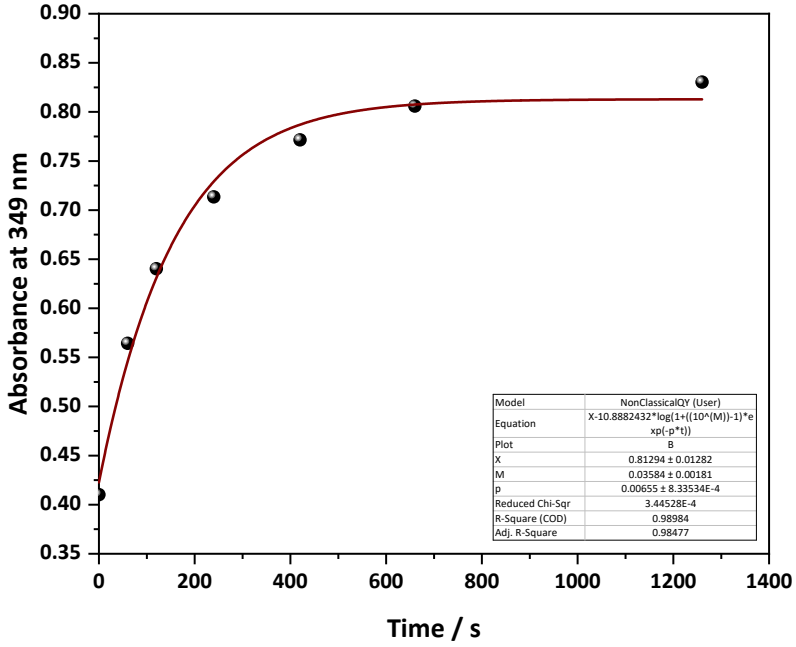

Figure S45: Evolution of the absorbance at λ = 349 nm during irradiation at λ_{ex} = 436 nm of **(*Z*)-AzoLA** in chloroform as function of time and corresponding fit using Maafi and Brown[2,3] photo-kinetic model.

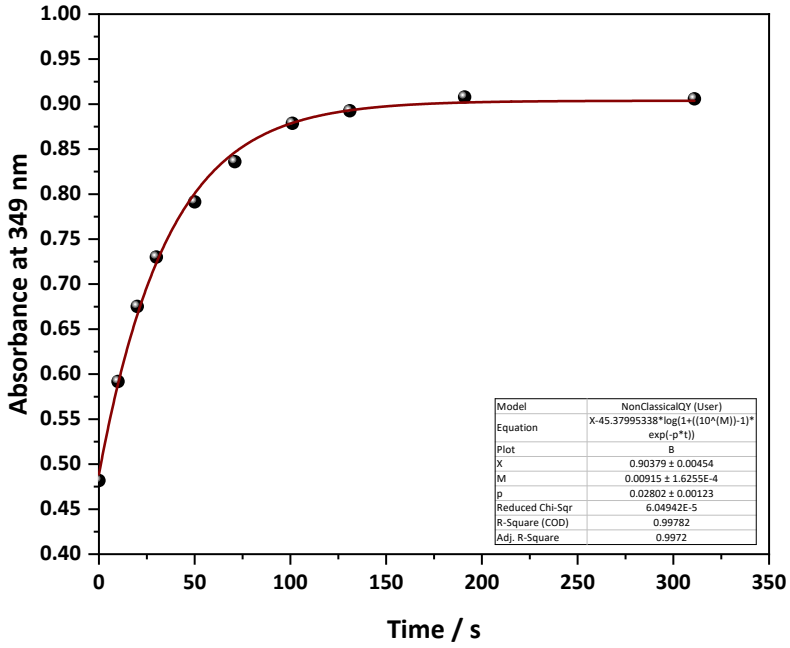

Figure S46: Evolution of the absorbance at λ = 349 nm during irradiation at λ_{ex} = 533 nm of **(*Z*)-AzoLA** in chloroform as function of time and corresponding fit using Maafi and Brown[2,3] photo-kinetic model.

NMR study of CIS-QDs and AzoAA interaction

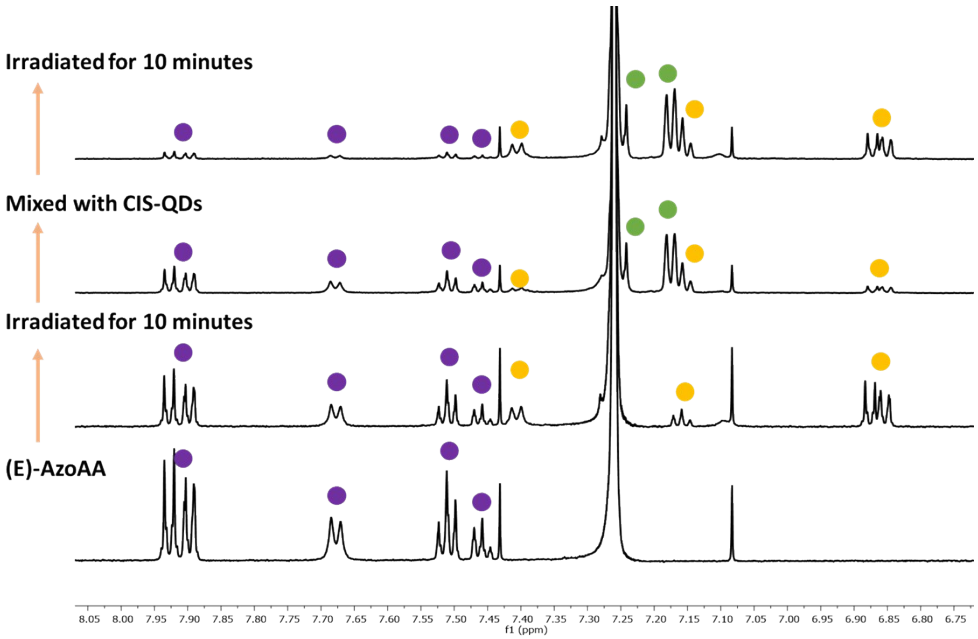

Figure S47: NMR spectra of **AzoAA** before and after mixture with **CIS-QDs** at different irradiation times. Irradiation was performed at 365 nm. D_1 was adjusted to 10 s to account for the hindered mobility of **(*Z*)-AzoAA** when associated with **CIS-QDs**, which leads to a decrease in T_2 relaxation, as reported in previous examples.[4,5] **(*E*)-AzoAA** (●), **(*Z*)-AzoAA** (●), **CIS⊂(*Z*)-AzoAA** (●).

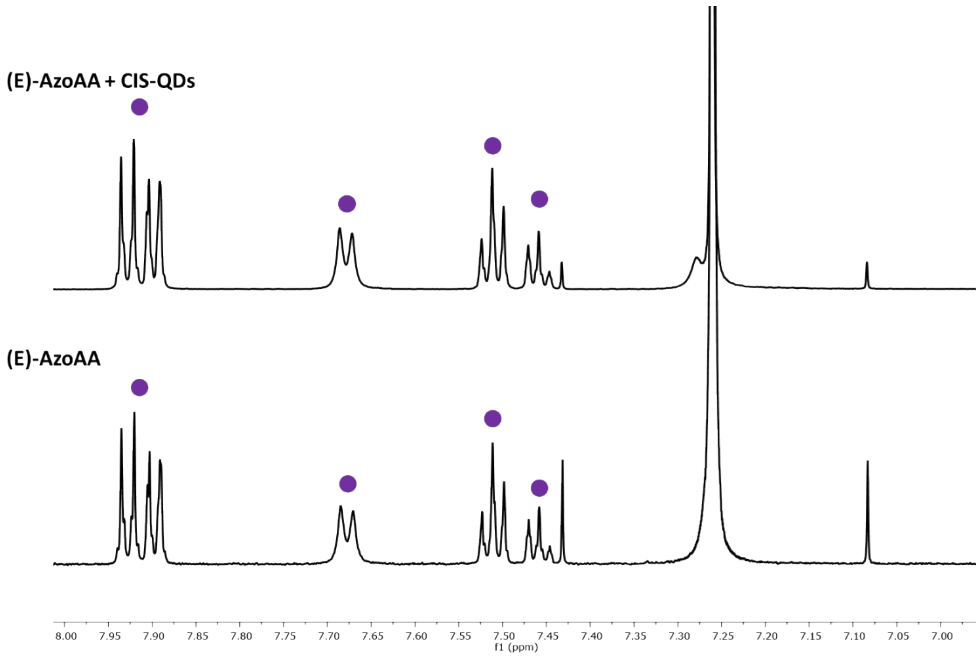

Figure S48: NMR spectra of **(*E*)-AzoAA** and a mixture of **(*E*)-AzoAA** and **CIS-QDs**. **(*E*)-AzoAA** ( ).

Thermal back isomerisation

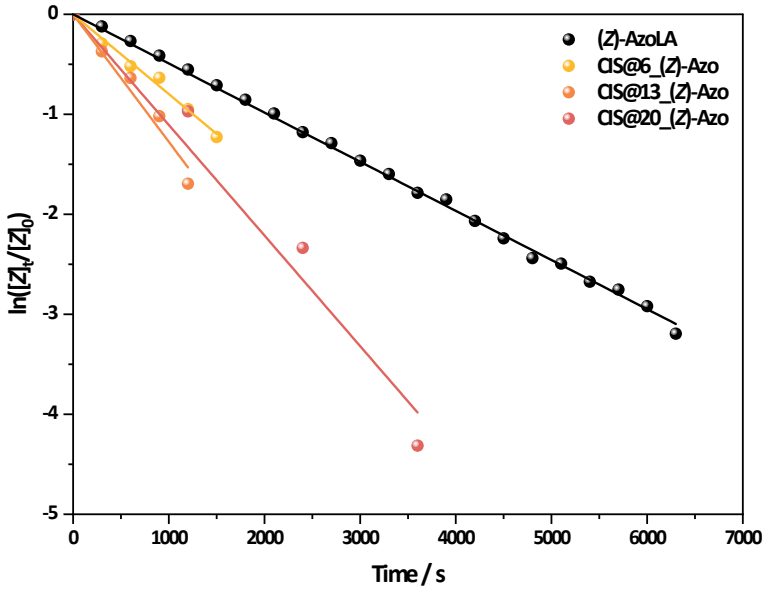

Figure S49: Relative pseudo-first order rate constants for the thermal isomerization (measured at 349 nm) of **(*Z*)-AzoLA** (black), **CIS@6_(*Z*)-Azo** (yellow), **CIS@13_(*Z*)-Azo** (orange), **CIS@20_(*Z*)-Azo** (red) in DMF at T = 70°C.

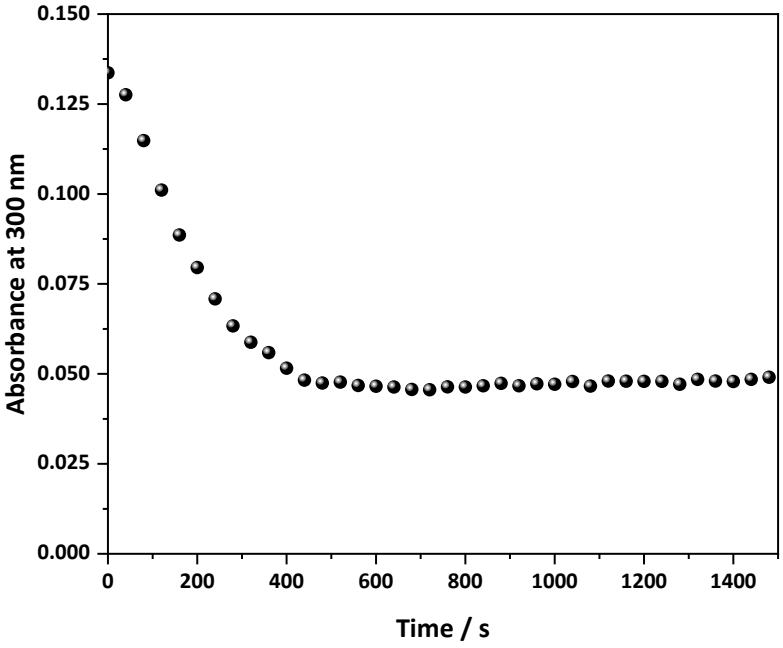

Figure S50: Evolution of the absorbance at 300 nm at T = 25 °C over the time after mixing a chloroform solution of **(*Z*)-AzoAA** ($1x10^{-5}$ M) with a solution of CIS-QDs ($1x10^{-6}$ M) in chloroform.

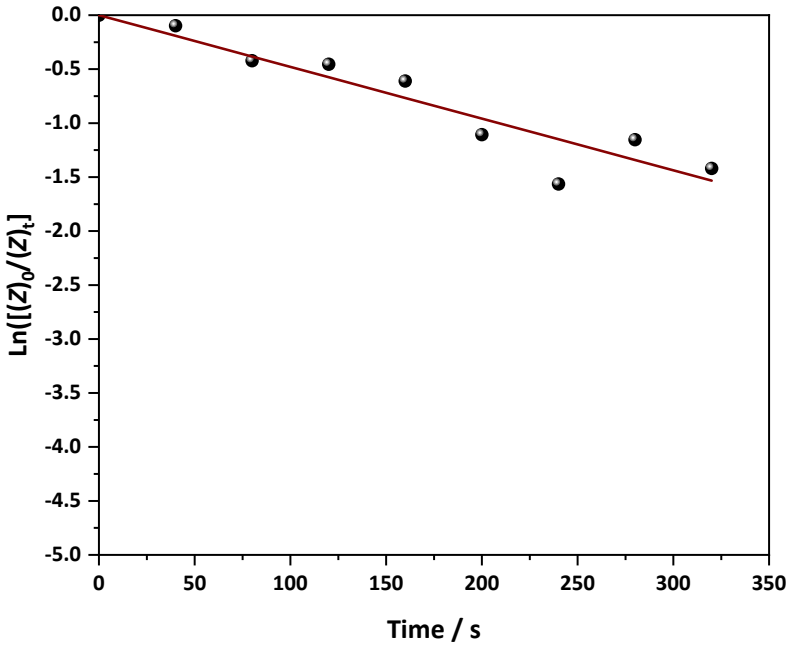

Figure S51: Relative pseudo-first order rate constant for the complexation of **(*Z*)-AzoAA** with CIS-QDs (measured at 300 nm) in chloroform at T = 25°C.

Elemental Analysis

A sample of CIS-QDs (0.2 mL) was purified by precipitation in acetone. The resulting powder was digested for 72 hours in 3 mL of nitric acid 7M.

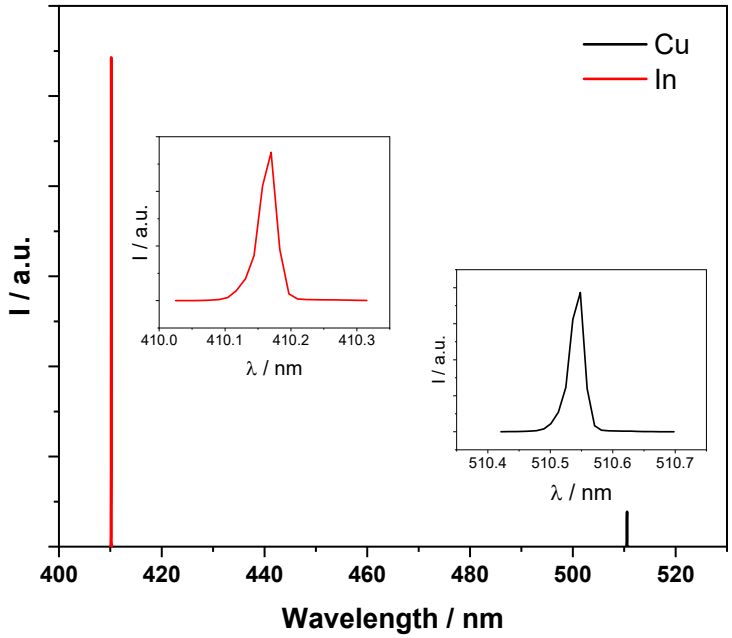

Figure S52: Detected atomic emission of ions resulting from the digestion of **CIS-QDs**.

Table S3: Detected metal concentration of the digested sample of **CIS-QDs** and calculated Cu:In molar ratio.

In / ppm	Cu / ppm	Cu:In molar ratio
68.72	36.25	0.97

References

1 M. Booth, A. P. Brown, S. D. Evans and K. Critchley, *Chem Mater*, 2012, **24**, 2064–2070.
2 M. Maafi and R. G. Brown, *J. Photochem. Photobiol. Chem.*, 2007, **187**, 319–324.
3 M. Maafi, *Front. Chem.*, 2023, **11**, 1233151–1233173.
4 Z. Hens, *Acc. Chem. Res.*, 2023, **56**, 1623–1633.
5 J. De Roo, N. Yazdani, E. Drijvers, A. Lauria, J. Maes, J. S. Owen, I. Van Driessche, M. Niederberger, V. Wood, J. C. Martins, I. Infante and Z. Hens, *Chem. Mater.*, 2018, **30**, 5485–5492.